

**Electromagnetic Propagation Through a Slotted Wall Inserted in a
Parallel-Plate Waveguide**

BY

GIORGIO CARNEVALI

B.S, Universita' Politecnica delle Marche, Ancona, Italy, 2016

THESIS

Submitted as partial fulfillment of the requirements
for the degree of Master of Science in Electrical and Computer Engineering
in the Graduate College of the
University of Illinois at Chicago, 2019

Chicago, Illinois

Defense Committee:

Piergiorgio L.E. Uslenghi, Chair and Advisor

Danilo Erricolo

Giuseppe Vecchi, Politecnico di Torino

ACKNOWLEDGMENTS

At the end (for now) of my academic career as a student, I look back and I see a fundamental period of my life, that I'll remember forever. I see a period of formation, of experience, of many sacrifices, reached goals, good times and also bad times. I would really like to thank all the people who have accompanied me in this period, from Turin, to Chicago. That city was my dream when I was a Bachelor student and I'm glad that I could participate in the UIC project and live this experience. I am so grateful to my advisor, Professor Uslenghi, whose explanations about electromagnetic scattering and very complex mathematical concepts were precious to me to complete this thesis. Thanks to him also for giving me this important project and for helping me when I was in a troubled period. To professor Erricolo, who was so kind to me, helping me with the numerical calculations every time I needed it and special thanks to professor Vecchi for accepting me as student, from Politecnico. Thanks to my girlfriend Erica, for her love to me when I was so far away from her, she helped me to follow my dream, I was not always the man she deserved, but I love her. I thank my friends and travel mates from Ancona to Turin, Camillo Di Antonio, Kevin Luciani and Stefano Luna, my UIC colleagues and friends Giorgio Bonomo, Marco Montagna, Francesca Pistilli, Francesco D'Amico and Francesco Marcantoni. Thanks to my family for their unconditional support and trust in me.

GC

TABLE OF CONTENTS

<u>CHAPTER</u>		<u>PAGE</u>
1	INTRODUCTION	1
2	HISTORY AND DESCRIPTION OF THE PROBLEM	3
3	SOLUTION FOR THE TEM MODE	6
3.1	Normal incidence, E-polarization solution (TEM mode)	6
3.1.1	Limit cases	11
3.1.2	Surface current densities	12
3.2	H-polarization solution	15
4	SOLUTION FOR THE TM MODES	19
4.1	Oblique incidence, E-polarization (TM modes)	19
4.2	Surface current densities	26
5	SOLUTION FOR THE TE MODES	30
5.1	Oblique incidence, H-polarization (TE modes)	30
5.2	Surface current densities	35
6	NUMERICAL RESULTS	38
6.1	Surface current densities for TEM case	39
6.2	Surface current densities for TM case	39
6.3	Surface current densities for TE case	41
7	CONCLUSIONS	55
	CITED LITERATURE	56
	VITA	57

LIST OF FIGURES

<u>FIGURE</u>		<u>PAGE</u>
1	Slotted wall inserted in a parallel plate waveguide in with reference system	5
2	Semielliptical cavity	5
3	parallel plate waveguide in reference system	29
4	Plane waves components of E-polarization solution	29
5	Plane waves components of H-polarization solution	37
6	TEM mode: amplitude and phase of J_{z1} for $\zeta = 0.5$:left side for $c = (0.1; 1.0; 5.0)$, right side for $c = (0.5; 2.0; 10.0)$	42
7	TEM mode: amplitude and phase of J_{z2} for $\zeta = 0.5$: left side for $c = (0.1; 1.0; 5.0)$,right side for $c = (0.5; 2.0; 10.0)$	43
8	TEM mode: amplitude and phase of J_{z1} (left side) and J_{z2} (right side) for $\zeta = (0.5; 1.0; 2.0)$ and $c = 0.5$	44
9	TM mode: amplitude of J_{z1} and J_{z2} w.r.t ξ and $\frac{z}{b}$ with $\zeta = 0.5$ and $\gamma = \frac{1}{2\sqrt{2}}$	45
10	TM mode: amplitude of J_{z1} and J_{z2} w.r.t ξ and $\frac{z}{b}$ with $\zeta = 1$ and $\gamma = \frac{2}{\sqrt{2}}$	45
11	TM mode: amplitude of J_{z1} and J_{z2} w.r.t ξ and $\frac{z}{b}$ with $\zeta = 2$ and $\gamma = \frac{10}{\sqrt{2}}$	46
12	TM mode: amplitude and phase of $J_{\xi 1}$ for $\zeta = 0.5$: left side for $\gamma = (\frac{\sqrt{2}}{20}; \frac{\sqrt{2}}{2}; \frac{5}{\sqrt{2}})$, right side for $\gamma = (\frac{\sqrt{2}}{4}; \sqrt{2}; \frac{10}{\sqrt{2}})$	47
13	TM mode:Amplitude and phase of $J_{\xi 2}$ for $\zeta = 0.5$: left side for $\gamma = (\frac{\sqrt{2}}{20}; \frac{\sqrt{2}}{2}; \frac{5}{\sqrt{2}})$,right side for $\gamma = (\frac{\sqrt{2}}{4}; \sqrt{2}; \frac{10}{\sqrt{2}})$	48
14	TM mode: amplitude and phase of $J_{\xi 1}$ (left side) and $J_{\xi 2}$ (right side) for $\zeta = (0.5; 1.0; 2.0)$, $\gamma = \frac{\sqrt{2}}{2}$, $\eta = \frac{\sqrt{2}}{2}$	49
15	TM mode: amplitude and phase of J_{v1} for $\zeta = 0.5$: left side for $\gamma = (\frac{\sqrt{2}}{20}; \frac{\sqrt{2}}{2}; \frac{5}{\sqrt{2}})$, right side for $\gamma = (\frac{\sqrt{2}}{4}; \sqrt{2}; \frac{10}{\sqrt{2}})$	50
16	TM mode: Amplitude and phase of J_{v2} for $\zeta = 0.5$: left side for $\gamma = (\frac{\sqrt{2}}{20}; \frac{\sqrt{2}}{2}; \frac{5}{\sqrt{2}})$,right side for $\gamma = (\frac{\sqrt{2}}{4}; \sqrt{2}; \frac{10}{\sqrt{2}})$	51
17	TM mode: amplitude and phase of J_{v1} (left side) and J_{v2} (right side) for $\zeta = (0.5; 1.0; 2.0)$, $\gamma = \frac{\sqrt{2}}{2}$, $\eta = \frac{\sqrt{2}}{2}$	52
18	TE mode: amplitude of J_{z1} and J_{z2} w.r.t ξ and $\frac{z}{b}$ with $\zeta = 0.5$ and $\gamma = \frac{1}{2\sqrt{2}}$	53
19	TE mode: amplitude of J_{z1} and J_{z2} w.r.t ξ and $\frac{z}{b}$ with $\zeta = 1$ and $\gamma = \frac{2}{\sqrt{2}}$	53

LIST OF FIGURES (continued)

FIGURE

PAGE

20	TE mode: amplitude of J_{z1} and J_{z2} w.r.t ξ and $\frac{z}{b}$ with $\zeta = 2$ and $\gamma = \frac{5}{\sqrt{2}}$	54
----	--	----

LIST OF ABBREVIATIONS

TEM	Transverse Electromagnetic
TE	Transverse Electric
TM	Transverse magnetic
PEC	Perfect Electric Conductor

SUMMARY

In this thesis a new electromagnetic scattering problem is solved analytically. The structure considered is a parallel-plate waveguide in which a slotted wall is inserted. Exact expressions of the electromagnetic field and surface current densities in the whole structure, for the characteristic modes of the parallel-plate waveguide (TEM mode, TE and TM modes) are theoretically evaluated. Numerical calculations of the surface current densities on the metallic posts and parallel plates are performed too, with the assistance of Fortran 90 subroutines.

CHAPTER 1

INTRODUCTION

A new scattering problem is presented in this thesis. In order to solve it analytically, the well known concepts of the electromagnetic field in a parallel-plate waveguide are used, together with the general results obtained in previous works by professor Uslenghi [1], [2] about exact solutions to scattering problems in particular structures, with cavities and metal edges. The entire analysis is conducted in phasor domain, with time dependence factor $e^{j\omega t}$, omitted throughout. The structure, described in detail in Chapter 2, is a parallel plate waveguide with a slotted wall inserted; all the metallic parts are assumed to be PEC and the dielectric materials, both on one side and the other of the slotted wall, isorefractive. In Chapter 3 the scattering of a wave with normal incidence to the slotted wall is solved; the analysis is performed for an E-polarized field, that in the structure corresponds to the TEM mode of the parallel-plate waveguide, but also for an H-polarized field since its expression is needed for the TE mode analysis (done in Chapter 5). The scattering analysis of TM modes is performed in Chapter 4 and likewise for TE modes in Chapter 5, the results of normal incidence are used, together with the formulas of [2] concerned with the oblique incidence of a wave on a structure truncated by a metal plane. In Chapter 6 numerical results are presented for the surface current densities on the metal slotted wall in the three cases and, in addition, on the metal parallel plates for the TM case. All of that thanks to the code developed by professor Erricolo on the computation of Mathieu functions, that was used in addition to a short part of code that puts together

the values of Mathieu functions needed in order to evaluate all the surface currents derivated theoretically.

CHAPTER 2

HISTORY AND DESCRIPTION OF THE PROBLEM

In Figure 1 is shown the three-dimensional structure analyzed. The metal parallel-plates extend to the infinity along the x direction and stand respectively on the plane $z = 0$ and $z = b$. The electromagnetic wave, in case of normal incidence (both for E and H polarization) propagates towards the negative y -direction; same thing for TE and TM modes with the difference that the propagation vector presents a component along the direction z , alternatively positive and negative.

The slotted wall is in the plane $y = 0$, the dielectric materials in the two parts of the structure, divided by the wall, are isotropic, linear and homogeneous. They have respectively permittivity ϵ_1 and ϵ_2 , permeability μ_1 and μ_2 and intrinsic impedances Z_1 and Z_2 . It's necessary that the two materials are isorefractive to perform the analysis, otherwise the canonical solutions obtained by professor Uslenghi [1] couldn't be used. Isorefractivity [3] means that:

$$\epsilon_1\mu_1 = \epsilon_2\mu_2$$

but in general

$$\left(Z_1 = \sqrt{\frac{\mu_1}{\epsilon_1}} \right) \neq \left(Z_2 = \sqrt{\frac{\mu_2}{\epsilon_2}} \right)$$

The slotted wall is treated like a particular case of an elliptic cavity, shown in Figure 2.

To perform the derivations it's therefore necessary to introduce the elliptic coordinates (u, v, z) , that are related to the Cartesian system by

$$x = \frac{d}{2} \cosh u \cos v$$

$$y = \frac{d}{2} \sinh u \sin v$$

$$z = z$$

where $0 < u < \infty$ and $0 < v < 2\pi$. Three other variables are introduced for simplicity:

$\xi = \cosh u$, $\eta = \cos v$ and $c = \frac{kd}{2}$ where d is the interfocal distance and k is the wave number.

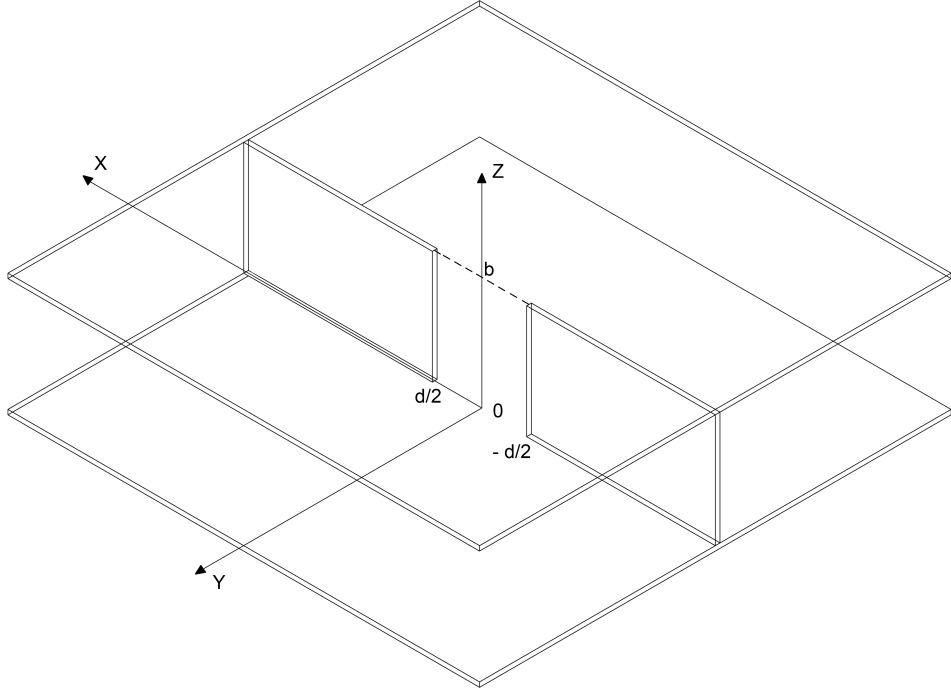


Figure 1: Slotted wall inserted in a parallel plate waveguide in with reference system

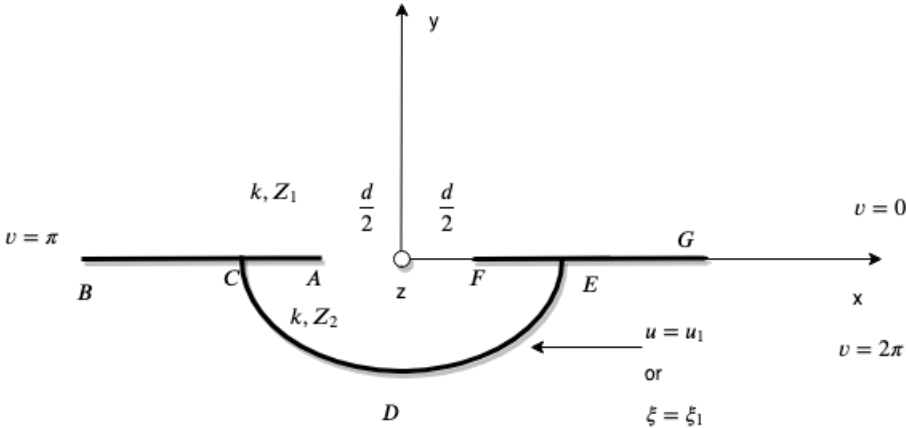


Figure 2: Semielliptical cavity

CHAPTER 3

SOLUTION FOR THE TEM MODE

3.1 Normal incidence, E-polarization solution (TEM mode)

It's considered a plane wave, normally incident on the slotted wall

$$\underline{E}^i = \hat{z}E_{1z}$$

$$E_{1z} = e^{jky}$$

with the wave number $k = \omega\sqrt{\epsilon_{1,2}\mu_{1,2}}$.

According to the electromagnetic theory [4], the electric field, incident in general with an angle ϕ_0 with respect to the negative x -axis, can be expanded in a series of elliptic-cylinder wave functions

$$E_{1z}^i = \sqrt{8\pi} \sum_{l=0}^{\infty} (j)^l \left[\frac{1}{N_l^{(e)}(c)} Re_l^{(1)}(c, \xi) Se_l(c, \eta) Se_l(c, \cos\phi_0) + \frac{1}{N_l^{(o)}(c)} Ro_l^{(1)}(c, \xi) So_l(c, \eta) So_l(c, \cos\phi_0) \right] \quad (3.1)$$

where $Re_l^{(1)}$, $Ro_l^{(1)}$ are even and odd Mathieu functions of the first kind, Se_l , So_l are even and odd angular Mathieu functions and $N_l^{(e),(o)}(c)$ are normalization coefficients, all according to the Stratton notation [4].

In this case of normal incidence, according to the current reference system, $\phi_0 = \frac{\pi}{2}$.

Considering the properties of the even Mathieu angular functions:

$$Se_m(c, \eta) \Big|_{v=\pi \pm v_0} = (-1)^m Se_m(c, \eta) \Big|_{v=v_0}$$

For $v_0 = \frac{\pi}{2}$:

$$Se_m(c, 0) = (-1)^m Se_m(c, 0)$$

$$Se_{2l+1}(c, 0) = 0$$

In the same way for odd Mathieu angular functions

$$So_m(c, \eta) \Big|_{v=\pi \pm v_0} = \pm (-1)^m So_m(c, \eta) \Big|_{v=v_0}$$

For $v_0 = \frac{\pi}{2}$:

$$So_m(c, 0) = -(-1)^m So_m(c, 0)$$

$$So_{2l}(c, 0) = 0$$

After these considerations the incident electric field can be written in the following way:

$$E_{1z}^i = \sqrt{8\pi} \sum_{l=0}^{\infty} (-1)^l \left[\frac{1}{N_{2l}^{(e)}(c)} Re_{2l}^{(1)}(c, \xi) Se_{2l}(c, \eta) Se_{2l}(c, 0) + \frac{j}{N_{2l+1}^{(o)}(c)} Ro_{2l+1}^{(1)}(c, \xi) So_{2l+1}(c, \eta) So_{2l+1}(c, 0) \right] \quad (3.2)$$

The electric field that would be reflected by the metal plane $y = 0$ is

$$E_{1z}^r = -\sqrt{8\pi} \sum_{l=0}^{\infty} (-1)^l \left[\frac{1}{N_{2l}^{(e)}(c)} Re_{2l}^{(1)}(c, \xi) Se_{2l}(c, \eta) Se_{2l}(c, 0) - \frac{j}{N_{2l+1}^{(o)}(c)} Ro_{2l+1}^{(1)}(c, \xi) So_{2l+1}(c, \eta) So_{2l+1}(c, 0) \right] \quad (3.3)$$

So that, the sum of the two terms is

$$E_{1z}^{i+r} = 4\sqrt{2\pi} \sum_{l=0}^{\infty} j(-1)^l \frac{1}{N_{2l+1}^{(o)}(c)} Ro_{2l+1}^{(1)}(c, \xi) So_{2l+1}(c, \eta) So_{2l+1}(c, 0) \quad (3.4)$$

and the diffracted electric field is

$$E_{1z}^d = 4\sqrt{2\pi} \sum_{l=0}^{\infty} \frac{(-1)^l}{N_{2l+1}^{(o)}(c)} a_l^{(h)}(c) Ro_{2l+1}^{(4)}(c, \xi) So_{2l+1}(c, \eta) So_{2l+1}(c, 0) \quad (3.5)$$

Where $Ro_{2l+1}^{(4)}$ is the radial Mathieu function of 4th type is used for the satisfaction of the radiation condition at infinity, since it asymptotically tends to zero.

The total electric field in the first medium is the sum of the previous terms and therefore can be expressed as follows

$$E_{1z}^{(e)} = 4\sqrt{2\pi} \sum_{l=0}^{\infty} \frac{j(-1)^l}{N_{2l+1}^{(o)}} \left[Ro_{2l+1}^{(1)}(c, \xi) + a_l^{(e)}(c) Ro_{2l+1}^{(4)}(c, \xi) \right] So_{2l+1}(c, \eta) So_{2l+1}(c, 0) \quad (3.6)$$

In the second medium, inside the cavity, the expression for the total electric field is:

$$E_{2z}^{(e)} = 4\sqrt{2\pi} \sum_{l=0}^{\infty} \frac{j(-1)^l}{N_{2l+1}^{(o)}} b_l^{(e)}(c) \left[\frac{Ro_{2l+1}^{(4)}(c, \xi_1)}{Ro_{2l+1}^{(1)}(c, \xi_1)} Ro_{2l+1}^{(1)}(c, \xi) - Ro_{2l+1}^{(4)}(c, \xi) So_{2l+1}(c, \eta) So_{2l+1}(c, 0) \right] \quad (3.7)$$

The magnetic field components are obtained in the following way:

$$H_{(1,2)\xi}^{(e)} = \frac{j}{cZ_1 \sqrt{\xi^2 - \eta^2}} \frac{\partial}{\partial v} E_{(1,2)z} \quad (3.8)$$

$$H_{(1,2)v}^{(e)} = \frac{-j}{cZ_1 \sqrt{\xi^2 - \eta^2}} \frac{\partial}{\partial u} E_{(1,2)z} \quad (3.9)$$

The unknown coefficients $a_l^{(e)}(c)$ and $b_l^{(e)}(c)$ are determined by imposing the boundary condition of continuity of the total tangential electric and magnetic field on the interface $u = 0$, or analogally, $\xi = 1$. The boundary conditions, according to the current reference system, can be written:

$$E_{1z}^{(e)} = E_{2z}^{(e)} \Big|_{u=0} \quad (3.10)$$

Where $So_{2l+1}(c, \eta) \Big|_{v=2\pi-v_0} = -So_{2l+1}(c, \eta) \Big|_{v=v_0}$

$$H_{1v}^{(e)} = -H_{2v}^{(e)} \Big|_{u=0} \quad (3.11)$$

i.e. $H_{1x}^{(e)} = H_{2x}^{(e)} \Big|_{u=0}$

Notice that in equations (Equation 3.10) and (Equation 3.11), $\eta = \cos v|_{y=0+} = \cos 2\pi - v|_{y=0-}$

From (Equation 3.6) and (Equation 3.7) into (Equation 3.10):

$$b_l^{(e)}(c) = a_l^{(e)}(c) \quad (3.12)$$

Where

$$Ro_{2l+1}^{(1)}(c) = 0 \quad (3.13)$$

was used. Starting from the (Equation 3.9) into (Equation 3.11), using (Equation 3.6), (Equation 3.7) and (Equation 3.12): the following result is obtained:

$$a_l^{(e)}(c) = \frac{1}{\zeta \frac{Ro_{2l+1}^{(4)}(c, \xi_1)}{Ro_{2l+1}^{(1)}(c, \xi_1)} - (1 + \zeta) \frac{Ro_{2l+1}^{(4)'}(c, 1)}{Ro_{2l+1}^{(1)'}(c, 1)}} \quad (3.14)$$

where $\zeta = \frac{Z_1}{Z_2}$ and the apex prime means "derivative with respect to u"

3.1.1 Limit cases

The first limit case is if medium 2 is a PEC, that means there's no cavity, $Z_2 = 0$ hence $\zeta \rightarrow \infty$ and

$$a_l^{(e)}(c) \Big|_{Z_2=0} = b_l^{(e)}(c) \Big|_{Z_2=0} = 0$$

The second limit case is the one of interest, it means if the cavity $\xi = \xi_1$ of is removed to infinity, therefore that medium 2 fills a half space and since is not an active medium and ($Im [c] < 0$). P hysically corresponds to the slotted wall.

Since $\lim_{\xi_1 \rightarrow \infty} Ro_{2l+1}^{(4)}(c, \xi_1) = 0$

$$a_l^{(e)}(c) \Big|_{\xi_1 \rightarrow \infty} = b_l^{(e)}(c) \Big|_{\xi_1 \rightarrow \infty} = -\frac{Ro_{2l+1}^{(1)'}(c, 1)}{(1 + \xi)Ro_{2l+1}^{(4)'}(c, 1)} \quad (3.15)$$

This result leads to the following expression for the electric field components:

$$E_{1z}^{(e)} \Big|_{\xi \rightarrow \infty} = 4\sqrt{2\pi} \sum_{l=0}^{\infty} \frac{j(-1)^l}{N_{2l+1}^o(c)} \left[Ro_{2l+1}^{(1)}(c, \xi) - \frac{Ro_{2l+1}^{(1)'}(c, 1)}{(1 + \zeta)Ro_{2l+1}^{(4)'}(c, 1)} Ro_{2l+1}^{(4)}(c, \xi) \right] So_{2l+1}(c, \eta) So_{2l+1}(c, 0) \quad (3.16)$$

$$E_{2z}^{(e)} \Big|_{\xi \rightarrow \infty} = 4\sqrt{2\pi} \sum_{l=0}^{\infty} \frac{j(-1)^l}{N_{2l+1}^o(c)} \frac{Ro_{2l+1}^{(1)'}(c, 1)}{(1 + \zeta)Ro_{2l+1}^{(4)'}(c, 1)} Ro_{2l+1}^{(4)}(c, \xi) So_{2l+1}(c, \eta) So_{2l+1}(c, 0) \quad (3.17)$$

Notice that the diffracted electric field in the first and the transmitted electric field into medium 1 are symmetrical with respect to the plane $y = 0$:

$$\left(E_{1z}^d \Big|_{\xi_1 \rightarrow \infty} \right)_{\xi=\xi_0, v=v_0} = \left(E_{2z}^{(e)} \Big|_{\xi_1 \rightarrow \infty} \right)_{\xi=\xi_0, v=(2\pi-v_0)} \quad (3.18)$$

3.1.2 Surface current densities

The surface current densities depends on the magnetic field components at the surface, according to the electromagnetic theory:

$$\underline{J} = \hat{n} \times \underline{H}$$

So in the different parts of the structure, referring to Figure 2 the current densities are defined:

$$FG(v = 0); \hat{n} = \hat{v}; \quad \underline{J}_1^{(e)} = -H_{1\xi}|_{v=0} \hat{z} \quad (3.19)$$

$$AB(v = \pi); \hat{n} = -\hat{v}; \quad \underline{J}_1^{(e)} = H_{1\xi}|_{v=\pi} \hat{z} \quad (3.20)$$

$$FE(v = 2\pi); \hat{n} = -\hat{v}; \quad \underline{J}_2^{(e)} = -H_{2\xi}|_{v=2\pi} \hat{z} \quad (3.21)$$

$$AC(v = \pi); \hat{n} = \hat{v}; \quad \underline{J}_2^{(e)} = -H_{2\xi}|_{v=\pi} \hat{z} \quad (3.22)$$

$$CDE(\xi = \xi_1); \hat{n} = -\hat{u}; \quad \underline{J}_1^{(e)} = -H_{2v}|_{\xi=\xi_1} \hat{z} \quad (3.23)$$

As consequence:

$$J_{1z}^{(e)} \Big|_{v=0} = \frac{4}{cZ_1} \sqrt{\frac{2\pi}{\xi^2 - 1}} \sum_{l=0}^{\infty} \frac{(-1)^l}{N_{2l+1}^{(o)}} So_{2l+1}(c, 0) \left[Ro_{2l+1}^{(1)}(c, \xi) + a_l^{(e)}(c) Ro_{2l+1}^{(4)}(c, \xi) \right] \quad (3.24)$$

$$J_{1z}^{(e)} \Big|_{v=\pi} = \frac{4}{cZ_1} \sqrt{\frac{2\pi}{\xi^2 - 1}} \sum_{l=0}^{\infty} \frac{(-1)^l}{N_{2l+1}^{(o)}} So_{2l+1}(c, 0) \left[Ro_{2l+1}^{(1)}(c, \xi) + a_l^{(e)}(c) Ro_{2l+1}^{(4)}(c, \xi) \right] = J_{1z}^{(e)} \Big|_{v=0} \quad (3.25)$$

$$J_{2z}^{(e)} \Big|_{v=2\pi} = \frac{-4}{cZ_2} \sqrt{\frac{2\pi}{\xi^2 - 1}} \sum_{l=0}^{\infty} \frac{(-1)^l}{N_{2l+1}^{(o)}} a_l^{(e)}(c) So_{2l+1}(c, 0) \left[\frac{Ro_{2l+1}^{(4)}(c, \xi_1)}{Ro_{2l+1}^{(1)}(c, \xi_1)} Ro_{2l+1}^{(1)}(c, \xi) - Ro_{2l+1}^{(4)}(c, \xi) \right] \quad (3.26)$$

$$\begin{aligned} J_{2z}^{(e)} \Big|_{v=\pi} &= \frac{-4}{cZ_2} \sqrt{\frac{2\pi}{\xi^2 - 1}} \sum_{l=0}^{\infty} \frac{(-1)^l}{N_{2l+1}^{(o)}} a_l^{(e)}(c) So_{2l+1}(c, 0) \left[\frac{Ro_{2l+1}^{(4)}(c, \xi_1)}{Ro_{2l+1}^{(1)}(c, \xi_1)} Ro_{2l+1}^{(1)}(c, \xi) - Ro_{2l+1}^{(4)}(c, \xi) \right] = \\ &= J_{2z}^{(e)} \Big|_{v=2\pi} \end{aligned} \quad (3.27)$$

$$J_{2z}^{(e)} \Big|_{u=u_1} = \frac{-4j}{cZ_2} \sqrt{\frac{2\pi}{\xi^2 - 1}} \sum_{l=0}^{\infty} \frac{(-1)^l}{N_{2l+1}^{(o)}} a_l^{(e)}(c) \frac{So_{2l+1}(c, 0)}{Ro_{2l+1}^{(1)}(c, \xi_1)} So_{2l+1}(c, \eta) \quad (3.28)$$

Where in (Equation 3.28) the Wronskian property for radial Mathieu functions was used, that

is:

$$Re, o_l^{(1)}(c, \xi) \frac{\partial}{\partial v} Re, o_l^{(4)}(c, \xi) - Re, o_l^{(4)}(c, \xi) \frac{\partial}{\partial v} Re, o_l^{(1)}(c, \xi) = -j \quad (3.29)$$

On the concave corners C and E:

$$J_{2z}^{(e)} \Big|_{v=\pi; u=u_1} = J_{2z}^{(e)} \Big|_{v=2\pi; u=u_1} = J_{2z}^{(e)} \Big|_{v=\pi, 2\pi; u=u_1} = 0 \quad (3.30)$$

The current densities near the sharp edges A and F, using (Equation 3.13) it's seen that

$$\left\{ \begin{array}{l} J_{1z}^{(e)} \Big|_{v=0; \xi \rightarrow 1} \simeq \frac{K}{Z_1 \sqrt{\xi^2 - 1}} \\ J_{2z}^{(e)} \Big|_{v=2\pi; \xi \rightarrow 1} \simeq \frac{K}{Z_2 \sqrt{\xi^2 - 1}} \end{array} \right. \quad (3.31)$$

Where K is a constant.

Set $\xi = 1 + \delta$, where $\delta \ll 1$, then $\frac{1}{\sqrt{\xi^2 - 1}} \simeq \frac{1}{\sqrt{2\delta}}$; For $v = 0, 2\pi$, $x = \frac{d}{2}\xi = \frac{d}{2}(1 + \delta) = \frac{d}{2} + w$, where $w = x - \frac{d}{2} = \frac{d}{2}\delta$ is the distance from the edge F.

The currents in (Equation 3.31) diverge as $\frac{1}{\sqrt{w}}$ as the edge is approached, as expected.

A similar reasoning rules also for the edge A, this means that the edge condition at A and F is satisfied.

The surface currents, considering no closed cavity ($\xi_1 \rightarrow \infty$) :

$$J_{1z}^{(e)} \Big|_{v=0,\pi} = \frac{4}{cZ_1} \sqrt{\frac{2\pi}{\xi_1^2 - 1}} \sum_{l=0}^{\infty} \frac{j(-1)^l}{N_{2l+1}^o} So_{2l+1}(c, 0) \left[Ro_{2l+1}^{(1)}(c, \xi) - \frac{Ro_{2l+1}^{(1)'}(c, 1)}{(1 + \xi)Ro_{2l+1}^{(4)'}(c, 1)} Ro_{2l+1}^{(4)}(c, \xi) \right] \quad (3.32)$$

$$J_{2z}^{(e)} \Big|_{v=\pi,2\pi} = \frac{-4}{cZ_2} \sqrt{\frac{2\pi}{\xi_1^2 - 1}} \sum_{l=0}^{\infty} \frac{j(-1)^l}{N_{2l+1}^o} So_{2l+1}(c, 0) \frac{Ro_{2l+1}^{(1)'}(c, 1)}{(1 + \xi)Ro_{2l+1}^{(4)'}(c, 1)} Ro_{2l+1}^{(4)}(c, \xi) \quad (3.33)$$

The surface currents expressed in (Equation 3.32) and (Equation 3.33) are numerically calculated in Chapter 6.

3.2 H-polarization solution

The method of analysis for an H-polarized field is analog to the E-polarization.

An incident magnetic field is given:

$$\underline{H}^i = \hat{z} H_{1z}$$

$$H_{1z} = e^{jky}$$

The expression can be expanded in Mathieu functions

$$H_{1z}^i = \sqrt{8\pi} \sum_{l=0}^{\infty} (j)^m \left[\frac{1}{N_l^{(e)}(c)} Re_l^{(1)}(c, \xi) Se_l(c, \eta) Se_l(c, \cos\phi_0) + \frac{1}{N_l^{(o)}(c)} Ro_l^{(1)}(c, \xi) So_l(c, \eta) So_l(c, \cos\phi_0) \right] \quad (3.34)$$

Given $\phi = \frac{\pi}{2}$ and considering the properties of the even and odd Mathieu angular functions given in the previous section the magnetic field can be rewritten:

$$H_{1z}^i = \sqrt{8\pi} \sum_{l=0}^{\infty} (-1)^l \left[\frac{1}{N_{2l}^{(e)}} Re_{2l}^{(1)}(c, \xi) Se_{2l}(c, \eta) Se_{2l}(c, 0) + \frac{j}{N_{2l+1}^{(o)}} Ro_{2l+1}^{(1)}(c, \xi) So_{2l+1}(c, \eta) So_{2l+1}(c, 0) \right] \quad (3.35)$$

The magnetic field that would be reflected by the metal plane $y = 0$ is

$$H_{1z}^r = \sqrt{8\pi} \sum_{l=0}^{\infty} (-1)^l \left[\frac{1}{N_{2l}^{(e)}(c)} Re_{2l}^{(1)}(c, \xi) Se_{2l}(c, \eta) Se_{2l}(c, 0) - \frac{j}{N_{2l+1}^{(o)}(c)} Ro_{2l+1}^{(1)}(c, \xi) So_{2l+1}(c, \eta) So_{2l+1}(c, 0) \right] \quad (3.36)$$

So that the sum of the two terms is

$$H_{1z}^{i+r} = 4\sqrt{2\pi} \sum_{l=0}^{\infty} (-1)^l \frac{1}{N_{2l}^{(e)}(c)} Re_{2l}^{(1)}(c, \xi) Se_{2l}(c, \eta) Se_{2l}(c, 0) \quad (3.37)$$

and the diffracted magnetic field

$$H_{1z}^d = 4\sqrt{2\pi} \sum_{l=0}^{\infty} \frac{(-1)^l}{N_{2l}^{(e)}(c)} a_l^{(h)}(c) Re_{2l}^{(4)}(c, \xi) Se_{2l}(c, \eta) Se_{2l}(c, 0) \quad (3.38)$$

Where the radial Mathieu function of 4th type is used for the satisfaction of the radiation condition at infinity. Therefore the electric field in the first medium is:

$$H_{1z}^{(h)} = H_{1z}^i + H_{1z}^r + H_{1z}^d$$

That leads to:

$$H_{1z}^{(h)} = 4\sqrt{2\pi} \sum_{l=0}^{\infty} \frac{(-1)^l}{N_{2l}^{(c)}} \left[Re_{2l}^{(1)}(c, \xi) + a_l^{(h)}(c) Re_{2l}^{(4)}(c, \xi) \right] Se_{2l}(c, \eta) Se_{2l}(c, 0) \quad (3.39)$$

Whereas the total magnetic field inside the cavity is:

$$H_{2z}^{(h)} = 4\sqrt{2\pi} \sum_{l=0}^{\infty} \frac{(-1)^l}{N_{2l}^{(e)}(c)} b_l^{(h)}(c) \left[\frac{Re_{2l}^{(4)'}(c, \xi_1)}{Re_{2l}^{(1)'}(c, \xi_1)} Re_{2l}^{(1)}(c, \xi) - Re_{2l}^{(4)}(c, \xi) \right] Se_{2l}(c, \eta) Se_{2l}(c, 0) \quad (3.40)$$

To find the coefficients $a_l^{(h)}(c)$ and $b_l^{(h)}(c)$ the boundary conditions at the interface between the two mediums are applied, in the same way of the E-polarization case:

$$H_{1z}^{(h)} = H_{2z}^{(h)} \Big|_{u=0} \quad (3.41)$$

$$E_{1v}^{(e)} = -E_{2v}^{(e)} \Big|_{u=0} \quad (3.42)$$

Considering that:

$$E_v = \frac{jZ}{c\sqrt{\xi^2 - \eta^2}} \frac{\partial H_z}{\partial u}$$

Starting from (Equation 3.42) and using the following property

$$\frac{\partial}{\partial u} Re_l^{(1)}(c, \xi) \Big|_{u=0} = 0$$

the result obtained is:

$$a_l^{(h)}(c) = \frac{1}{\zeta} b_l^{(h)}(c) \quad (3.43)$$

From (Equation 3.41), using (Equation 3.43):

$$a_l^{(h)}(c) = \frac{1}{\zeta \left(\frac{Re_{2l}^{(4)}(c, \xi_1)}{Re_{2l}^{(1)}(c, \xi_1)} \right) - (1 + \zeta) \left(\frac{Re_{2l}^{(4)}(c, 1)}{Re_{2l}^{(1)}(c, 1)} \right)} \quad (3.44)$$

Finally considering the cavity removed to infinity ($\xi_1 \rightarrow \infty$)

$$a_l^{(h)}(c) = \frac{1}{\zeta} b_l^{(h)}(c) = - \frac{Re_{2l}^{(1)}(c, 1)}{(1 + \zeta) Re_{2l}^{(4)}(c, 1)} \quad (3.45)$$

CHAPTER 4

SOLUTION FOR THE TM MODES

4.1 Oblique incidence, E-polarization (TM modes)

The propagation of an electromagnetic wave in the parallel plate waveguide, according to the current reference system that fits with the one of the elliptical cavity from [1], shown in Figure 1 is analyzed. The position of the parallel plates and the direction of the wave, with respect to the system is indicated in Figure 3, notice that the infinite direction is along the x -axis, that means in the solution of the Maxwell equations to carry out the expression of the field in propagation in the waveguide, no dependance on the x directions is considered, $\frac{\partial}{\partial x} = 0$. Solving Maxwell's equations in the parallel-plate waveguide with this reference system leads to two systems of equations, the first for the TM solution (E-polarization) and the second for the TE one (H-polarization).

$$\left\{ \begin{array}{l} \frac{\partial^2 H_x}{\partial y^2} + \frac{\partial^2 H_x}{\partial z^2} + \omega^2 \mu \epsilon H_x = 0 \\ \frac{\partial H_x}{\partial z} = j\omega \epsilon E_y \\ -\frac{\partial H_x}{\partial y} = j\omega \epsilon E_z \end{array} \right. \quad (4.1)$$

$$\begin{cases} \frac{\partial^2 E_x}{\partial y^2} + \frac{\partial^2 E_x}{\partial z^2} + \omega^2 \mu \epsilon E_x = 0 \\ \frac{\partial E_x}{\partial z} = -j\omega \mu H_y \\ -\frac{\partial E_x}{\partial y} = -j\omega \mu H_z \end{cases} \quad (4.2)$$

The solution to the differential equations system (Equation 4.1), it means E-polarized field for a wave propagating along the negative y -axis, according to the reference system can be written as:

$$\begin{cases} H_x^{(e)} = -Y \cos(\beta z) e^{jk_t y} \\ E_y^{(e)} = \frac{\beta}{jk} \sin(\beta z) e^{jk_t y} \\ E_z^{(e)} = \frac{k_t}{k} \cos(\beta z) e^{jk_t y} \end{cases} \quad (4.3)$$

where:

$Y = \sqrt{\frac{\epsilon}{\mu}}$ is the intrinsic admittance of the medium;

$\beta^2 + k_t^2 = k^2$, k_t is the wave number in the propagation direction;

$\beta = \frac{n\pi}{b}$, from the boundary condition of zero electric field on the PEC plates;

$n = (0, 1, 2, \dots)$ is a number, that defines the mode of propagation.

The electromagnetic field can be schematized as two plane waves, both propagating in the negative y direction but in opposite z directions. This is analytically and geometrically shown respectively in (Equation 4.4) and in Figure 4.

$$\begin{cases} H_x^{(e)} = -\frac{Y}{2} \left(e^{jk_t y + \beta z} + e^{jk_t y - \beta z} \right) \\ E_y^{(e)} = -\frac{\beta}{2k} \left(e^{jk_t y + \beta z} - e^{jk_t y - \beta z} \right) \\ E_z^{(e)} = \frac{k_t}{2k} \left(e^{jk_t y + \beta z} + e^{jk_t y - \beta z} \right) \end{cases} \quad (4.4)$$

The first plane wave is propagating in direction $\hat{k}_1^i = -\frac{k_t}{k}\hat{y} - \frac{\beta}{k}\hat{z}$ forming the angle θ_{01} with the negative z -axis, whereas the second plane is propagating in direction $\hat{k}_2^i = -\frac{k_t}{k}\hat{y} + \frac{\beta}{k}\hat{z}$ forming the angle θ_{02} with the negative z -axis.

$$\begin{cases} \cos \theta_{01} = \frac{\beta}{k} \\ \sin \theta_{01} = \frac{k_t}{k} \end{cases} \quad (4.5)$$

$$\begin{cases} \cos \theta_{02} = -\frac{\beta}{k} \\ \sin \theta_{02} = \frac{k_t}{k} \end{cases} \quad (4.6)$$

The positive direction of x -axis enters the plane yz , in fact the $H_x^{(e)}$ component, for both plane waves is negative and has opposite direction; the direction of $E^{(e)}$ is clearly shown in Figure 4.

Starting from the TEM-solution results for E-polarization and using the method used in [?] for the general three-dimensional oblique problem the electromagnetic field expression can be developed in the following way: From (Equation 3.6) and (Equation 3.7) using (Equation 3.12):

$$E_\nu^{(e)} = \hat{z} \Big|_{2D} = \hat{z} E_{\nu z}^{(e)} \Big|_{2D} = \hat{z} U_\nu^{(e)}(\xi, \eta; c) \quad (4.7)$$

where $\nu = (1, 2)$ and, from

$$U_1^{(e)}(\xi, \eta; c) = 4\sqrt{2\pi} \sum_{l=0}^{\infty} \frac{(-1)^l}{N_{2l+1}^{(o)}} \left[Ro_{2l+1}^{(1)}(c, \xi) + a_l^{(e)}(c) Ro_{2l+1}^{(4)}(c, \xi) \right] So_{2l+1}(c, \eta) So_{2l+1}(c, 0) \quad (4.8)$$

$$U_2^{(e)}(\xi, \eta; c) = 4\sqrt{2\pi} \sum_{l=0}^{\infty} \frac{j(-1)^l}{N_{2l+1}^{(o)}} b_l^{(e)}(c) \left[\frac{Ro_{2l+1}^{(4)}(c, \xi_1)}{Ro_{2l+1}^{(1)}(c, \xi_1)} Ro_{2l+1}^{(1)}(c, \xi) - Ro_{2l+1}^{(4)}(c, \xi) So_{2l+1}(c, \eta) \times \right. \\ \left. \times So_{2l+1}(c, 0) \right] \quad (4.9)$$

Applying the equations (22), (23) in [2], dividing each component by 2 and adding them it's obtained:

$$\underline{E}_l^{(e)} = \frac{1}{2} \sum_{\nu=1}^2 \left[-\frac{2}{k} \cot \theta_{0\nu} \sin kz \cos \theta_{0\nu} \nabla_t U_l^{(e)}(\xi, \eta; c \sin \theta_{0\nu}) + 2 \sin \theta_{0\nu} \cos kz \cos \theta_{0\nu} U_l^{(e)}(\xi, \eta; c \sin \theta_{0\nu}) \hat{z} \right] \quad (4.10)$$

$$\underline{E}_l^{(e)} = \frac{1}{2} \sum_{\nu=1}^2 -\frac{2jY_2}{k \sin \theta_{0\nu}} \cos kz \cos \theta_{0\nu} (\hat{z} \times \nabla_t) U_l^{(e)}(\xi, \eta; c \sin \theta_{0\nu}) \quad (4.11)$$

Considering $l = (1; 2)$ and the same for ν :

$$k \sin \theta_{01} = k \sin \theta_{02} = k_t$$

$$c \sin \theta_{01} = c \sin \theta_{02} = \frac{k_t d}{2} = \gamma$$

$$k \cos \theta_{01} = \beta$$

$$k \cos \theta_{02} = -\beta$$

$$\frac{\cot \theta_{01}}{k} = \frac{\beta}{k k_t} = -\frac{\cot \theta_{02}}{k}$$

Therefore:

$$\underline{E}_l^{(e)} = \frac{-2\beta}{k k_t} \sin \beta z \nabla_t U_l^{(e)}(\xi, \eta; \gamma) + \frac{2k_t}{k} \cos \beta z U_l^{(e)}(\xi, \eta; \gamma) \hat{z} \quad (4.12)$$

$$\underline{H}_l^{(e)} = \frac{-2jY_l}{k_t} \cos \beta z (\hat{z} \times \nabla_t) U_l^{(e)}(\xi, \eta; \gamma) \quad (4.13)$$

In elliptic-cylinder coordinates:

$$\nabla_t = \frac{2}{d\sqrt{\xi^2 - \eta^2}} \left(\hat{u} \frac{\partial}{\partial u} + \hat{v} \frac{\partial}{\partial v} \right)$$

$$\hat{z} \times \nabla_t = \frac{2}{d\sqrt{\xi^2 - \eta^2}} \left(-\hat{u} \frac{\partial}{\partial v} + \hat{v} \frac{\partial}{\partial u} \right)$$

That leads to the following results for the electric and magnetic field in the first medium:

$$\begin{aligned}
\underline{E}_1^{(e)} = & -\frac{8\beta}{k\gamma} \sqrt{\frac{2\pi}{\xi^2 - \eta^2}} \sin \beta z \sum_{l=0}^{\infty} \frac{j(-1)^l}{N_{2l+1}^{(o)}(\gamma)} So_{2l+1}(\gamma, 0) \left\{ \hat{u} \times \left[Ro^{(1)}{}_{2l+1}(\gamma, \xi) + \right. \right. \\
& + a_l^{(e)}(\gamma) Ro^{(4)}{}_{2l+1}(\gamma, \xi) \left. \right] So_{2l+1}(\gamma, \eta) + \hat{v} \left[Ro_{2l+1}^{(1)}(\gamma, \xi) + a_l^{(e)}(\gamma) Ro_{2l+1}^{(4)}(\gamma, \xi) \right] \times \\
& \times \frac{\partial}{\partial v} So_{2l+1}(\gamma, \eta) \left. \right\} + 8\sqrt{2\pi} \frac{k_t}{k} \cos \beta z \hat{z} \sum_{l=0}^{\infty} \frac{(-1)^l}{N_{2l+1}^{(o)}} \left[Ro_{2l+1}^{(1)}(\gamma, \xi) + \right. \\
& + a_l^{(e)}(\gamma) Ro_{2l+1}^{(4)}(\gamma, \xi) \left. \right] So_{2l+1}(\gamma, \eta) So_{2l+1}(\gamma, 0)
\end{aligned} \tag{4.14}$$

$$\begin{aligned}
\underline{H}_1^{(e)} = & \frac{8jY_1}{\gamma} \sqrt{\frac{2\pi}{\xi^2 - \eta^2}} \cos \beta z \sum_{l=0}^{\infty} \frac{j(-1)^l}{N_{2l+1}^{(o)}(\gamma)} So_{2l+1}(\gamma, 0) \left\{ \hat{u} \times \left[Ro_{2l+1}^{(1)}(\gamma, \xi) + \right. \right. \\
& + a_l^{(e)}(\gamma) Ro_{2l+1}^{(4)}(\gamma, \xi) \left. \right] \frac{\partial}{\partial v} So_{2l+1}(\gamma, \eta) - \hat{v} \left[Ro_{2l+1}{}^{(1)}(\gamma, \xi) + \right. \\
& + a_l^{(e)}(\gamma) Ro_{2l+1}{}^{(4)}(\gamma, \xi) So_{2l+1}(\gamma, \eta) \left. \right\}
\end{aligned} \tag{4.15}$$

Where the apix "prime" means $\frac{\partial}{\partial u}$. Electric and magnetic field in the second medium are expressed as follows:

$$\begin{aligned}
\underline{E}_2^{(e)} = & -\frac{8\beta}{k\gamma} \sqrt{\frac{2\pi}{\xi^2 - \eta^2}} \sin \beta z \sum_{l=0}^{\infty} \frac{j(-1)^l}{N_{2l+1}^{(o)}(\gamma)} a_l^{(e)}(\gamma) S_{o_{2l+1}}(\gamma, 0) \left\{ \hat{u} \left[\frac{Ro_{2l+1}^{(4)}(\gamma, \xi_1)}{Ro_{2l+1}^{(1)}(\gamma, \xi_1)} Ro_{2l+1}^{(1)'}(\gamma, \xi) - \right. \right. \\
& \left. \left. - Ro_{2l+1}^{(4)'}(\gamma, \xi) \right] S_{o_{2l+1}}(\gamma, \eta) + \hat{v} \left[\frac{Ro_{2l+1}^{(4)}(\gamma, \xi_1)}{Ro_{2l+1}^{(1)}(\gamma, \xi_1)} Ro_{2l+1}^{(1)}(\gamma, \xi) - Ro_{2l+1}^{(4)}(\gamma, \xi_1) \right] \frac{\partial}{\partial v} S_{o_{2l+1}}(\gamma, \eta) \right\} \\
& + 8\sqrt{2\pi} \frac{k_t}{k} \cos \beta z \hat{z} \sum_{l=0}^{\infty} \frac{j(-1)^l a_l^{(e)}(\gamma)}{N_{2l+1}^{(o)}(\gamma)} \left[\frac{Ro_{2l+1}^{(4)}(\gamma, \xi_1)}{Ro_{2l+1}^{(1)}(\gamma, \xi_1)} Ro_{2l+1}^{(1)}(\gamma, \xi) - \right. \\
& \left. - Ro_{2l+1}^{(4)}(\gamma, \xi_1) \right] S_{o_{2l+1}}(\gamma, \eta) S_{o_{2l+1}}(\gamma, 0)
\end{aligned} \tag{4.16}$$

$$\begin{aligned}
\underline{H}_2^{(e)} = & \frac{8jY_1}{\gamma} \sqrt{\frac{2\pi}{\xi^2 - \eta^2}} \cos \beta z \sum_{l=0}^{\infty} \frac{j(-1)^l}{N_{2l+1}^{(o)}(\gamma)} a_l^{(e)}(\gamma) S_{o_{2l+1}}(\gamma, 0) \left\{ \hat{u} \left[\frac{Ro_{2l+1}^{(4)}(\gamma, \xi_1)}{Ro_{2l+1}^{(1)}(\gamma, \xi_1)} Ro_{2l+1}^{(1)}(\gamma, \xi) \right. \right. \\
& \left. \left. - Ro_{2l+1}^{(4)}(\gamma, \xi) \right] \frac{\partial}{\partial v} S_{o_{2l+1}}(\gamma, \eta) - \hat{v} \left[\frac{Ro_{2l+1}^{(4)}(\gamma, \xi_1)}{Ro_{2l+1}^{(1)}(\gamma, \xi_1)} Ro_{2l+1}^{(1)'}(\gamma, \xi) - Ro_{2l+1}^{(4)'}(\gamma, \xi) \right] S_{o_{2l+1}}(\gamma, \eta) \right\}
\end{aligned} \tag{4.17}$$

Following the same lead of the TEM solution it's possible to analyze the behavior of the electromagnetic field considering no cavity that means $\xi_1 \rightarrow \infty$, from (Equation 3.15):

$$a_l^{(e)}(\gamma) \Big|_{\xi_1 \rightarrow \infty} = b_l^{(e)}(\gamma) \Big|_{\xi_1 \rightarrow \infty} = -\frac{Ro_{2l+1}^{(1)'}(c, 1)}{(1 + \zeta) Ro_{2l+1}^{(4)'}(c, 1)}$$

Hence from (Equation 4.15) and (Equation 4.17):

$$\begin{aligned}
H_{1\xi}^{(e)} \Big|_{\xi_1 \rightarrow \infty} &= \frac{8jY_1}{\gamma} \sqrt{\frac{2\pi}{\xi^2 - \eta^2}} \cos \beta z \sum_{l=0}^{\infty} \frac{j(-1)^l}{N_{2l+1}(\gamma)} So_{2l+1}(\gamma, 0) \left[Ro_{2l+1}^{(1)}(\gamma, \xi) - \right. \\
&\quad \left. - \frac{Ro_{2l+1}^{(1)'}(c, 1)}{(1 + \zeta)Ro_{2l+1}^{(4)'}(c, 1)} Ro_{2l+1}^{(4)}(\gamma, \xi) \right] \frac{\partial}{\partial v} So_{2l+1}(\gamma, \eta)
\end{aligned} \tag{4.18}$$

$$\begin{aligned}
H_{2\xi}^{(e)} \Big|_{\xi_1 \rightarrow \infty} &= \frac{8jY_1}{\gamma} \sqrt{\frac{2\pi}{\xi^2 - \eta^2}} \cos \beta z \sum_{l=0}^{\infty} \frac{j(-1)^l}{N_{2l+1}(\gamma)} So_{2l+1}(\gamma, 0) \frac{Ro_{2l+1}^{(1)'}(c, 1)}{(1 + \zeta)Ro_{2l+1}^{(4)'}(c, 1)} So_{2l+1}(\gamma, 0) \times \\
&\quad \times Ro_{2l+1}^{(4)}(\gamma, \xi) \frac{\partial}{\partial v} So_{2l+1}(\gamma, \eta)
\end{aligned} \tag{4.19}$$

4.2 Surface current densities

Considering the same case of no closed cavity ($\xi_1 \rightarrow \infty$), according to the same reasoning of the TEM solution, the surface current densities in the two sides of the structure can be expressed as:

$$\begin{aligned}
J_{1z}^{(e)} \Big|_{v=0, \pi} &= \frac{8}{\gamma Z_1} \sqrt{\frac{2\pi}{\xi^2 - \eta^2}} \cos \beta z \sum_{l=0}^{\infty} \frac{j(-1)^l}{N_{2l+1}(\gamma)} So_{2l+1}(\gamma, 0) \left[Ro_{2l+1}^{(1)}(\gamma, \xi) - \right. \\
&\quad \left. - \frac{Ro_{2l+1}^{(1)'}(c, 1)}{(1 + \zeta)Ro_{2l+1}^{(4)'}(c, 1)} Ro_{2l+1}^{(4)}(\gamma, \xi) \right]
\end{aligned} \tag{4.20}$$

$$J_{2z}^{(e)} \Big|_{v=0,\pi} = -\frac{8}{\gamma Z_2} \sqrt{\frac{2\pi}{\xi^2 - \eta^2}} \cos \beta z \sum_{l=0}^{\infty} \frac{j(-1)^l}{N_{2l+1}(\gamma)} S_{o_{2l+1}}(\gamma, 0) \frac{Ro_{2l+1}^{(1)'}(\gamma, 1)}{(1 + \zeta) Ro_{2l+1}^{(4)'}(\gamma, 1)} Ro_{2l+1}^{(4)}(\gamma, \xi) \quad (4.21)$$

Since the propagation constant

$$k_t = \sqrt{k^2 - \beta} = \sqrt{k^2 - \left(\frac{n\pi}{b}\right)^2} = k \sqrt{1 - \left(\frac{n\pi}{kb}\right)^2}$$

is zero at cutoff frequency, to have propagation it's necessary that

$$kb > n\pi$$

It's arbitrarily chosen:

$$kb = \pi\sqrt{2} \quad (4.22)$$

So that only the lowest E-mode, for $n = 1$, that's the fundamental mode. Given this parameter it follows that:

$$\frac{\beta}{k} = \frac{k_t}{k} = \frac{1}{\sqrt{2}} = \sin \theta_{01} = \sin \theta_{02}$$

Hence $\gamma = c \frac{k_t}{k} = \frac{c}{\sqrt{2}}$ The current densities on the plate are evaluated too, in the case of no closed cavity ($\xi_1 \rightarrow \infty$):

$$\underline{J}^{(e)} \Big|_{z=0; \xi_1 \rightarrow \infty} = \hat{z} \times \underline{H}^{(e)} \Big|_{z=0; \xi_1 \rightarrow \infty} = \hat{z} \times \left[\hat{u} H_{\xi}^{(e)} \Big|_{z=0; \xi_1 \rightarrow \infty} + \hat{v} H_v^{(e)} \Big|_{z=0; \xi_1 \rightarrow \infty} \right]$$

$$\begin{aligned} J_{1\xi}^{(e)} \Big|_{v=0; \xi_1 \rightarrow \infty} &= -\frac{8}{\gamma Z_1} \sqrt{\frac{2\pi}{\xi^2 - \eta^2}} \sum_{l=0}^{\infty} \frac{j(-1)^l}{N_{2l+1}(\gamma)} S_{o_{2l+1}}(\gamma, 0) \left[Ro_{2l+1}^{(1)}(\gamma, \xi) - \right. \\ &\quad \left. - \frac{Ro_{2l+1}^{(1)}(c, 1)}{(1 + \zeta) Ro_{2l+1}^{(4)}(c, 1)} Ro_{2l+1}^{(4)}(\gamma, \xi) \right] S_{o_{2l+1}}(\gamma, \eta) \end{aligned} \quad (4.23)$$

$$J_{2\xi}^{(e)} \Big|_{v=0; \xi_1 \rightarrow \infty} = -\frac{8}{\gamma Z_2} \sqrt{\frac{2\pi}{\xi^2 - \eta^2}} \sum_{l=0}^{\infty} \frac{j(-1)^l}{N_{2l+1}(\gamma)} S_{o_{2l+1}}(\gamma, 0) \frac{Ro_{2l+1}^{(1)}(\gamma, 1)}{(1 + \zeta) Ro_{2l+1}^{(4)}(\gamma, 1)} Ro_{2l+1}^{(4)}(\gamma, \xi) \quad (4.24)$$

$$\begin{aligned} J_{1v}^{(e)} \Big|_{z=0; \xi_1 \rightarrow \infty} &= -\frac{8}{\gamma Z_1} \sqrt{\frac{2\pi}{\xi^2 - \eta^2}} \sum_{l=0}^{\infty} \frac{j(-1)^l}{N_{2l+1}(\gamma)} S_{o_{2l+1}}(\gamma, 0) \left[Ro_{2l+1}^{(1)}(\gamma, \xi) - \right. \\ &\quad \left. - \frac{Ro_{2l+1}^{(1)}(c, 1)}{(1 + \zeta) Ro_{2l+1}^{(4)}(c, 1)} Ro_{2l+1}^{(4)}(\gamma, \xi) \right] \frac{\partial}{\partial v} S_{o_{2l+1}}(\gamma, \eta) \end{aligned} \quad (4.25)$$

$$\begin{aligned} J_{2v}^{(e)} \Big|_{z=0; \xi_1 \rightarrow \infty} &= -\frac{8}{\gamma Z_2} \sqrt{\frac{2\pi}{\xi^2 - \eta^2}} \sum_{l=0}^{\infty} \frac{j(-1)^l}{N_{2l+1}(\gamma)} S_{o_{2l+1}}(\gamma, 0) \frac{Ro_{2l+1}^{(1)}(\gamma, 1)}{(1 + \zeta) Ro_{2l+1}^{(4)}(\gamma, 1)} \times \\ &\quad \times Ro_{2l+1}^{(4)}(\gamma, \xi) \frac{\partial}{\partial v} S_{o_{2l+1}}(\gamma, \eta) \end{aligned} \quad (4.26)$$

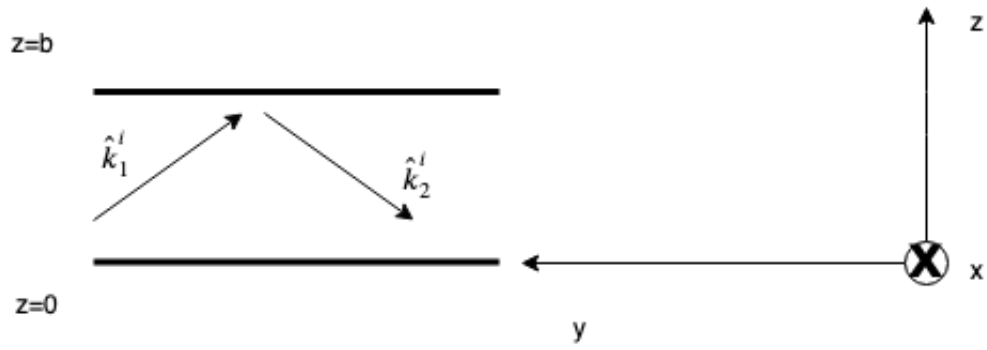


Figure 3: parallel plate waveguide in reference system

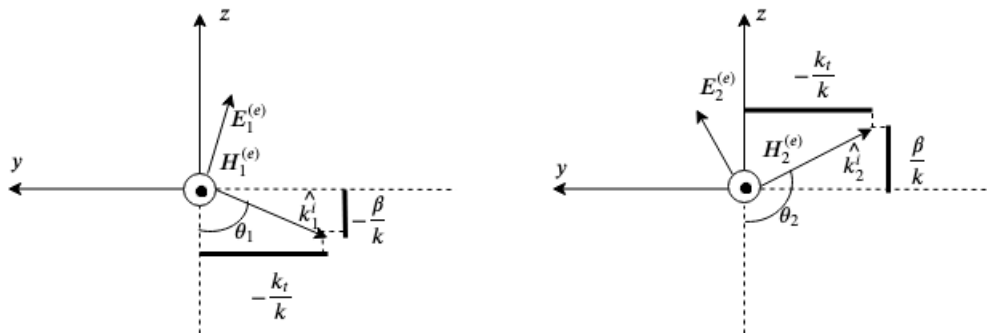


Figure 4: Plane waves components of E-polarization solution

CHAPTER 5

SOLUTION FOR THE TE MODES

5.1 Oblique incidence, H-polarization (TE modes)

The solution to the differential equations system (Equation 4.2) for a wave propagating along the negative y -axis, according to the reference system and considering the boundary condition of zero tangential electric field on both planes $z = 0$ and $z = d$ can be written as:

$$\begin{cases} E_x^{(h)} = \sin(\beta z)e^{jk_t y} \\ H_y^{(h)} = -\frac{\beta Y}{jk} \cos(\beta z)e^{jk_t y} \\ H_z^{(h)} = \frac{k_t Y}{k} \sin(\beta z)e^{jk_t y} \end{cases} \quad (5.1)$$

Following the same principles of E-polarization solution, the electromagnetic field can be schematized as two plane waves, both propagating in the negative y direction but in opposite z directions. This is analytically and geometrically shown in (Equation 5.2) and in Figure 5 .

$$\begin{cases} E_x^{(h)} = \frac{1}{2j} \left(e^{jk_t y + \beta z} - e^{jk_t y - \beta z} \right) \\ H_y^{(h)} = -\frac{\beta Y}{2jk} \left(e^{jk_t y + \beta z} + e^{jk_t y - \beta z} \right) \\ H_z^{(h)} = \frac{k_t Y}{2jk} \left(e^{jk_t y + \beta z} - e^{jk_t y - \beta z} \right) \end{cases} \quad (5.2)$$

In the same way of E-polarization the first plane wave is propagating in direction $\hat{k}_1^i = -\frac{k_t}{k}\hat{y} - \frac{\beta}{k}\hat{z}$ forming the angle θ_{01} with the negative z -axis, whereas the second plane is propagating in direction $\hat{k}_2^i = -\frac{k_t}{k}\hat{y} + \frac{\beta}{k}\hat{z}$ forming the angle θ_{02} with the negative z -axis. The positive direction of x -axis enters the plane yz , in fact the $E_x^{(h)}$ component, for the first plane wave is positive and has the same direction of x , whereas the second one is negative and has the opposite direction; the direction of $E^{(h)}$ is clearly shown in Figure 5, as well. The procedure to analyze the scattering solution follows the same principles of the E-polarized field. From (Equation 3.39) and (Equation 3.40), obtained in Chapter 3:

$$U_1^{(h)}(\xi, \eta; c) = 4\sqrt{2\pi} \sum_{l=0}^{\infty} \frac{(-1)^l}{N_{2l}^{(e)}} \left[Re_{2l}^{(1)}(c, \xi) + a_l^{(h)}(c) Re_{2l}^{(4)}(c, \xi) \right] Se_{2l}(c, \eta) Se_{2l}(c, 0) \quad (5.3)$$

$$U_2^{(h)}(\xi, \eta; c) = 4\sqrt{2\pi} \sum_{l=0}^{\infty} \frac{(-1)^l}{N_{2l}^{(e)}} b_l^{(h)}(c) \left[\frac{Re_{2l}^{(4)}(c, \xi_1)}{Re_{2l}^{(1)}(c, \xi_1)} Re_{2l}^{(1)}(c, \xi) - Re_{2l}^{(4)}(c, \xi) \right] Se_{2l}(c, \eta) Se_{2l}(c, 0) \quad (5.4)$$

Applying the formulas of paper [2] for H-polarization, for both the plane waves, dividing by two j and subtracting the components it's obtained:

$$E_l^{(h)} = \frac{1}{2j} \left(-\frac{2}{k \sin \theta_{01}} (\sin kz \cos \theta_{01}) (\hat{z} \times \nabla_t) U_l^{(h)}(\xi, \eta; c \sin \theta_{01}) \right) + \frac{1}{2j} \left(\frac{2}{k \sin \theta_{02}} (\sin kz \cos \theta_{01}) (\hat{z} \times \nabla_t) U_l^{(h)}(\xi, \eta; c \sin \theta_{02}) \right) \quad (5.5)$$

$$\begin{aligned}
H_l^{(h)} = & \frac{1}{2j} \left(\frac{2jY}{k} \cot \theta_{01} \cos kz \cos \theta_{01} \nabla_t U_l^{(h)}(\xi, \eta; c \sin \theta_{01}) + 2jY \sin \theta_{01} \sin kz \cos \theta_{01} U_l^{(h)}(\xi, \eta; c \sin \theta_{01}) \right) - \\
& - \frac{1}{2j} \left(\frac{2jY}{k} \cot \theta_{02} \cos kz \cos \theta_{02} \nabla_t U_l^{(h)}(\xi, \eta; c \sin \theta_{02}) - 2jY \sin \theta_{02} \sin kz \cos \theta_{02} U_l^{(h)}(\xi, \eta; c \sin \theta_{02}) \right)
\end{aligned} \tag{5.6}$$

Like in the E-polarization solution it rules that:

$$k \sin \theta_{01} = k \sin \theta_{02} = k_t$$

$$c \sin \theta_{01} = c \sin \theta_{02} = \frac{k_t d}{2} = \gamma$$

$$k \cos \theta_{01} = \beta$$

$$k \cos \theta_{02} = -\beta$$

$$\frac{\cot \theta_{01}}{k} = \frac{\beta}{kk_t} = -\frac{\cot \theta_{02}}{k}$$

Therefore in the first medium it's obtained

$$E_1^{(h)} = \frac{2j}{k_t} \sin \beta z (\hat{z} \times \nabla_t) U_l^{(h)}(\xi, \eta; \gamma) \tag{5.7}$$

$$H_l^{(h)} = \frac{2Y\beta}{kk_t} \cos \beta z \nabla_t U_1^{(h)}(\xi, \eta; \gamma) + \frac{2Yk_t}{k} \sin \beta z U_l^{(h)}(\xi, \eta; \gamma) \tag{5.8}$$

Equations (Equation 5.7) and (Equation 5.8), in a more general form are in a paper by Arora, Poort and Uslenghi, that is under review [5], [6].

The expressions in elliptic-cylinder coordinates can be expressed as follows:

$$E_1^{(h)} = \frac{8j}{\gamma} \sqrt{\frac{2\pi}{\xi^2 - \eta^2}} \sin \beta z \sum_{l=0}^{\infty} \frac{(-1)^l}{N_{2l}^{(e)}(\gamma)} S_{e2l}(\gamma, 0) \left\{ -\hat{u} \left[Re_{2l}^{(1)}(\gamma, \xi) + a_l^{(h)}(c) Re_{2l}^{(4)}(\gamma, \xi) \right] \frac{\partial}{\partial v} S_{e2l}(\gamma, \eta) + \hat{v} \left[Re_{2l}^{(1)\prime}(\gamma, \xi) + a_l^{(h)}(c) Re_{2l}^{(4)\prime}(\gamma, \xi) \right] S_{e2l}(\gamma, \eta) \right\} \quad (5.9)$$

$$H_1^{(h)} = \frac{8Y\beta}{k\gamma} \sqrt{\frac{2\pi}{\xi^2 - \eta^2}} \cos \beta z \sum_{l=0}^{\infty} \frac{(-1)^l}{N_{2l}^{(e)}(\gamma)} S_{e2l}(\gamma, 0) \left\{ \hat{u} \left[Re_{2l}^{(1)\prime}(\gamma, \xi) + a_l^{(h)}(\gamma) Re_{2l}^{(4)\prime}(\gamma, \xi) \right] S_{e2l}(\gamma, \eta) + \hat{v} \left[Re_{2l}^{(1)}(c, \xi) + a_l^{(h)}(\gamma) Re_{2l}^{(4)}(\gamma, \xi) \right] \frac{\partial}{\partial v} S_{e2l}(\gamma, \eta) \right\} + \hat{z} \frac{8Yk_t}{k} \sin \beta z \sqrt{2\pi} \sum_{l=0}^{\infty} \frac{(-1)^l}{N_{2l}^{(e)}} \left[Re_{2l}^{(1)}(\gamma, \xi) + a_l^{(h)}(c) Re_{2l}^{(4)}(\gamma, \xi) \right] S_{e2l}(\gamma, \eta) S_{e2l}(\gamma, 0) \quad (5.10)$$

Same equations rule for the second medium, but using $U_2^{(h)}$:

$$E_2^{(h)} = \frac{8j}{\gamma} \sqrt{\frac{2\pi}{\xi^2 - \eta^2}} \sin \beta z \sum_{l=0}^{\infty} \frac{(-1)^l}{N_{2l}^{(e)}(\gamma)} b_l^{(h)}(\gamma) S_{e2l}(\gamma, 0) \left\{ -\hat{u} \left[\frac{Re_{2l}^{(4)\prime}(\gamma, \xi_1)}{Re_{2l}^{(1)\prime}(\gamma, \xi_1)} Re_{2l}^{(1)}(\gamma, \xi) - Re_{2l}^{(4)}(\gamma, \xi) \right] \frac{\partial}{\partial v} S_{e2l}(\gamma, \eta) + \hat{v} \left[\frac{Re_{2l}^{(4)\prime}(\gamma, \xi_1)}{Re_{2l}^{(1)\prime}(\gamma, \xi_1)} Re_{2l}^{(1)\prime}(\gamma, \xi) - Re_{2l}^{(4)\prime}(\gamma, \xi) \right] S_{e2l}(\gamma, \eta) \right\} \quad (5.11)$$

$$\begin{aligned}
H_2^{(h)} = & \frac{8Y\beta}{k\gamma} \sqrt{\frac{2\pi}{\xi^2 - \eta^2}} \cos \beta z \sum_{l=0}^{\infty} \frac{(-1)^l}{N_{2l}^{(e)}(\gamma)} b_l^{(h)}(\gamma) S e_{2l}(\gamma, 0) \left\{ \hat{u} \left[\frac{R e_{2l}^{(4)'}(\gamma, \xi_1)}{R e_{2l}^{(1)'}(\gamma, \xi_1)} R e_{2l}^{(1)'}(\gamma, \xi) - \right. \right. \\
& \left. \left. - R e_{2l}^{(4)'}(\gamma, \xi) \right] S e_{2l}(\gamma, \eta) + \hat{v} \left[\frac{R e_{2l}^{(4)'}(\gamma, \xi_1)}{R e_{2l}^{(1)'}(\gamma, \xi_1)} R e_{2l}^{(1)'}(\gamma, \xi) - R e_{2l}^{(4)'}(\gamma, \xi) \right] \frac{\partial}{\partial v} S e_{2l}(\gamma, \eta) \right\} + \\
& + 8\sqrt{2\pi} \frac{Y k_t}{k} \sin \beta z \hat{z} \sum_{l=0}^{\infty} \frac{(-1)^l}{N_{2l}^{(e)}(\gamma)} b_l^{(h)}(\gamma) \left[\frac{R e_{2l}^{(4)'}(\gamma, \xi_1)}{R e_{2l}^{(1)'}(\gamma, \xi_1)} R e_{2l}^{(1)'}(\gamma, \xi) \right. \\
& \left. - R e_{2l}^{(4)'}(\gamma, \xi) \right] S e_{2l}(\gamma, \eta) S e_{2l}(\gamma, 0)
\end{aligned} \tag{5.12}$$

Considering no closed cavity case: ($\xi_1 \rightarrow \infty$), from Chapter 3 (Equation 4.3)

$$a_l^{(h)}(\gamma) = \frac{1}{\zeta} b_l^{(h)}(\gamma) = -\frac{R e_{2l}^{(1)'}(\gamma, 1)}{(1 + \zeta) R e_{2l}^{(4)'}(\gamma, 1)} \tag{5.13}$$

Follows that, from (Equation 5.10) and (Equation 5.12))

$$\begin{aligned}
H_{1\xi}^{(h)} \Big|_{\xi_1 \rightarrow \infty} = & \frac{8Y_1}{k\gamma} \sqrt{\frac{2\pi}{\xi^2 - \eta^2}} \cos \beta z \sum_{l=0}^{\infty} \frac{(-1)^l}{N_{2l}^{(e)}(\gamma)} S e_{2l}(\gamma, 0) \left[R e_{2l}^{(1)'}(\gamma, \xi) + \right. \\
& \left. + \frac{R e_{2l}^{(1)'}(\gamma, \xi_1)}{\zeta R e_{2l}^{(4)'}(\gamma, \xi_1)} R e_{2l}^{(4)'}(\gamma, \xi) \right] S e_{2l}(\gamma, \eta)
\end{aligned} \tag{5.14}$$

$$\begin{aligned}
H_{2\xi}^{(h)} \Big|_{\xi_1 \rightarrow \infty} = & \frac{8Y_2\beta}{k\gamma} \sqrt{\frac{2\pi}{\xi^2 - \eta^2}} \cos \beta z \sum_{l=0}^{\infty} \frac{(-1)^l}{N_{2l}^{(e)}(\gamma)} S e_{2l}(\gamma, 0) \left[R e_{2l}^{(1)'}(\gamma, \xi) - \right. \\
& \left. - \frac{R e_{2l}^{(1)'}(\gamma, \xi_1)}{R e_{2l}^{(4)'}(\gamma, \xi_1)} R e_{2l}^{(4)'}(\gamma, \xi) \right] S e_{2l}(\gamma, \eta)
\end{aligned} \tag{5.15}$$

5.2 Surface current densities

In the case of H-polarization the surface currents on the wall, considering the cavity removed to infinity:

$$J_{1z}^{(h)} \Big|_{\xi \rightarrow \infty; v=0} = -\frac{8Y_1\beta}{k\gamma} \sqrt{\frac{2\pi}{\xi^2-1}} \cos \beta z \sum_{l=0}^{\infty} \frac{(-1)^l}{N_{2l}^{(e)}(\gamma)} S e_{2l}(\gamma, 0) \left[R e_{2l}^{(1)}(\gamma, \xi) - \frac{R e_{2l}^{(1)}(\gamma, 1)}{(1+\zeta) R e_{2l}^{(4)}(\gamma, 1)} R e_{2l}^{(4)}(\gamma, \xi) \right] S e_{2l}(\gamma, 1) = J_{1z}^{(h)} \Big|_{\xi \rightarrow \infty; v=\pi} \quad (5.16)$$

$$J_{2z}^{(h)} \Big|_{\xi \rightarrow \infty; v=\pi} = -\frac{8Y_2\beta}{k\gamma} \sqrt{\frac{2\pi}{\xi^2-1}} \cos \beta z \sum_{l=0}^{\infty} \frac{(-1)^l}{N_{2l}^{(e)}(\gamma)} S e_{2l}(\gamma, 0) \times \frac{\zeta}{1+\zeta} \frac{R e_{2l}^{(1)}(\gamma, 1)}{R e_{2l}^{(4)}(\gamma, 1)} R e_{2l}^{(4)}(\gamma, \xi) S e_{2l}(\gamma, -1) = J_{2z}^{(h)} \Big|_{\xi \rightarrow \infty; v=2\pi} \quad (5.17)$$

Like for E-modes, $k_t = \sqrt{k^2 - \beta^2} = \sqrt{1 - \left(\frac{n\pi}{b}\right)^2}$ is zero at cut-off, so to have just the first H-mode in propagation it's needed that $kb > n\pi$. The same value chosen for E-modes $kb = \pi\sqrt{2}$, so that

$$\frac{\beta}{k} = \frac{k_t}{k} = \frac{1}{\sqrt{2}} = \sin \theta_{01}$$

$$\gamma = c \frac{k_t}{k} = \frac{c}{\sqrt{2}}$$

It's possible to express the surface current densities on the plates ($z = 0$), $\xi_1 \rightarrow \infty$:

$$\underline{J}^{(h)} \Big|_{z=0; \xi_1 \rightarrow \infty} = \hat{z} \times \underline{H}^{(h)} \Big|_{z=0; \xi_1 \rightarrow \infty} = \hat{z} \times \left[\hat{u} H_{\xi}^{(h)} \Big|_{z=0; \xi_1 \rightarrow \infty} + \hat{v} H_v^{(h)} \Big|_{z=0; \xi_1 \rightarrow \infty} \right]$$

$$\begin{aligned}
J_{1\xi}^{(h)} \Big|_{(z=0; \xi_1 \rightarrow \infty)} &= -H_{1v} \Big|_{(z=0; \xi_1 \rightarrow \infty)} = -\frac{8Y\beta}{k\gamma} \sqrt{\frac{2\pi}{\xi^2 - \eta^2}} \sum_{l=0}^{\infty} \frac{(-1)^l}{N_{2l}^{(e)}(\gamma)} Se_{2l}(\gamma, 0) \left[Re_{2l}^{(1)}(\gamma, \xi) - \right. \\
&\quad \left. - \frac{Re_{2l}^{(1)}(\gamma, 1)}{(1+\zeta)Re_{2l}^{(4)}(\gamma, 1)} Re_{2l}^{(4)}(\gamma, \xi) \right] \frac{\partial}{\partial v} Se_{2l}(\gamma, \eta)
\end{aligned} \tag{5.18}$$

$$\begin{aligned}
J_{2\xi}^{(h)} \Big|_{(z=0; \xi_1 \rightarrow \infty)} &= -H_{2v} \Big|_{(z=0; \xi_1 \rightarrow \infty)} = -\frac{8Y_2\beta}{k\gamma} \sqrt{\frac{2\pi}{\xi^2 - \eta^2}} \sum_{l=0}^{\infty} \frac{(-1)^l}{N_{2l}^{(e)}(\gamma)} Se_{2l}(\gamma, 0) \frac{\zeta}{1+\zeta} \times \\
&\quad \times \frac{Re_{2l}^{(1)}(\gamma, 1)}{Re_{2l}^{(4)}(\gamma, 1)} Re_{2l}^{(4)}(\gamma, \xi) \frac{\partial}{\partial v} Se_{2l}(\gamma, \eta)
\end{aligned} \tag{5.19}$$

$$\begin{aligned}
J_{1v}^{(h)} \Big|_{(z=0; \xi_1 \rightarrow \infty)} &= H_{1\xi} \Big|_{(z=0; \xi_1 \rightarrow \infty)} = \frac{8Y_1\beta}{k\gamma} \sqrt{\frac{2\pi}{\xi^2 - \eta^2}} \sum_{l=0}^{\infty} \frac{(-1)^l}{N_{2l}^{(e)}(\gamma)} Se_{2l}(\gamma, 0) \left[Re_{2l}^{(1)}(\gamma, \xi) - \right. \\
&\quad \left. - \frac{Re_{2l}^{(1)}(\gamma, 1)}{(1+\zeta)Re_{2l}^{(4)}(\gamma, 1)} Re_{2l}^{(4)}(\gamma, \xi) \right] Se_{2l}(\gamma, \eta)
\end{aligned} \tag{5.20}$$

$$\begin{aligned}
J_{2v}^{(h)} \Big|_{(z=0; \xi_1 \rightarrow \infty)} &= H_{2\xi} \Big|_{(z=0; \xi_1 \rightarrow \infty)} = \frac{8Y_2\beta}{k\gamma} \sqrt{\frac{2\pi}{\xi^2 - \eta^2}} \sum_{l=0}^{\infty} \frac{(-1)^l}{N_{2l}^{(e)}(\gamma)} Se_{2l}(\gamma, 0) \times \\
&\quad \times \frac{\zeta}{1+\zeta} \frac{Re_{2l}^{(1)}(\gamma, 1)}{Re_{2l}^{(4)}(\gamma, 1)} Re_{2l}^{(4)}(\gamma, \xi) Se_{2l}(\gamma, \eta)
\end{aligned} \tag{5.21}$$

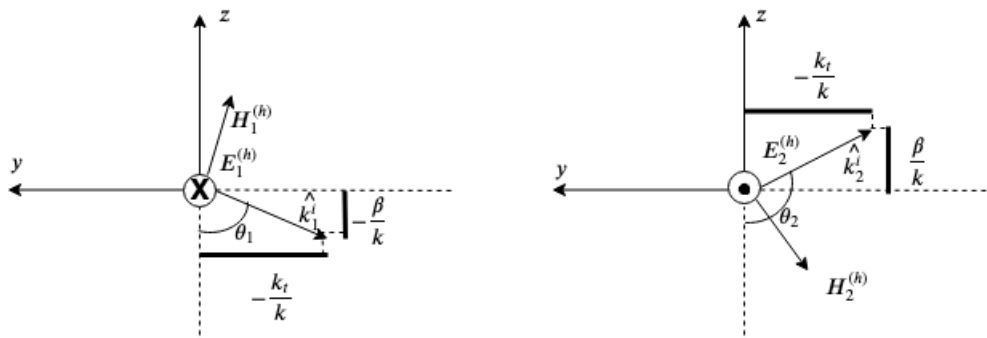


Figure 5: Plane waves components of H-polarization solution

CHAPTER 6

NUMERICAL RESULTS

The surface current densities, theoretically derived for the three cases, are numerically calculated in this section. To do this, an algorithm that produces as output the values of Mathieu functions for the given variables is required. This algorithm was developed by professor Erricolo and written in Fortran 90 language, the algorithm is explained in [7],[8],[9]. With the support of these Fortran subroutines, a short piece of code was written to put together all the terms needed to evaluate the various currents. Every result was written in a text file, read by the software Matlab2018b and displayed in different graphs, to show the variations of amplitude and phase of the surface current densities with respect to the impedances Z_1 , Z_2 , the c or γ parameter, and with the elliptic-cylinder coordinates ξ and η . The parameters given are:

$$Z_1 = Z_0 = 120\pi \Omega$$

with Z_0 that stands for the intrinsic impedance in vacuum.

$$\zeta = \frac{Z_1}{Z_2} = 0.5; 1.0; 2.0$$

$$c = 0.1; 0.5; 1.0; 2.0; 5.0; 10.0;$$

The graphs are plotted in function of ξ , over the range ($1 < \xi < 5$) with steps of $\Delta\xi = 0.1$.

6.1 Surface current densities for TEM case

Respectively in Figure 6 and Figure 7 are shown amplitude and phase of the surface current densities J_{z1} and J_{z2} derived in (Equation 3.32), (Equation 3.33), for $\zeta = 0.5$ and various values of c , indicated in the legend.

In Figure 8, amplitude and phase of J_{z1} and J_{z2} for the three given values of ζ are represented.

6.2 Surface current densities for TM case

The expressions for the first TM mode of J_{z1} and J_{z2} in (Equation 4.20) and (Equation 4.21) are practically similar to the TEM, but they are also function of the variable z through a cosine relation: $\cos \beta z = \cos \frac{\pi}{b} z$

So, some chosen cases are shown in Figure 9, Figure 10 and Figure 11 of the currents as functions of ξ and $\frac{z}{b}$, that means a 3D graph is needed to fully represent that double dependance.

For what concerns the surface current densities $J_{\xi 1}$ and $J_{\xi 2}$ of (Equation 4.23) and (Equation 4.24) they are evaluated with the same procedure of J_z in the TEM case, with the difference that they depend also on the variable η .

In Figure 12 and Figure 13 η is kept fixed at 1 and ζ is 0.5, moreover the parameter γ is nothing else but the c indicated in the legend divided by $\sqrt{2}$ as consequence of having chosen the first mode, see (Equation 4.22).

Since the results for the surface current densities $J_{\xi 1}$ and $J_{\xi 2}$ are evaluated just for 5 fixed values of η it's not possible to have a graph showing how they change keeping fixed ξ , γ and ζ for

every values of the angular coordinate. However the values of the currents for the η considered are:

$$\eta = (1; \frac{\sqrt{2}}{2}; 0; -\frac{\sqrt{2}}{2}; -1;)$$

$$|J_{\xi 1}| = (0.0030; 0.0051; 0; 0.0051; 0.0030)$$

$$\Phi(J_{\xi 1}) = (-0.3134; -0.1493; 0; -0.1493; -0.3134)$$

$$|J_{\xi 2}| = (0.0017; 0.0013; 0; 0.0013; 0.0017)$$

$$\Phi(J_{\xi 2}) = (0.9902; 0.9904; 0; 0.9904; 0.9902)$$

for $\zeta = 1, \gamma = \frac{\sqrt{2}}{2}, \xi = 3.0$.

Same kind of analysis is done for J_{v1} and J_{v2} of equations (Equation 4.25), (Equation 4.26). The graphs are reported in Figure 15, Figure 16 and Figure 17 for the same parameters of $J_{\xi 1}$ and $J_{\xi 2}$.

Like for the results of the surface current densities $J_{\xi 1}$ and $J_{\xi 2}$, the densities J_{v1} and J_{v2} are evaluated just for 5 fixed values of η , so it's not possible to have a graph showing how they change keeping fixed ξ , γ and ζ for every values of the angular coordinate. However the values of the currents, amplitude and phase for the η considered are:

$$\eta = (1; \frac{\sqrt{2}}{2}; 0; -\frac{\sqrt{2}}{2}; -1;)$$

$$|J_{v1}| = (0.0086; 0.0069; 0.0018; 0.0069; 0.0086)$$

$$\Phi(J_{v1}) = (-0.0776; -0.1298; -0.6622; -0.1298; -0.0776)$$

$$|J_{v2}| = (0.0016; 0.0021; 0.0026; 0.0021; 0.0016)$$

$$\Phi(J_{v2}) = (0.9838; 0.9837; 0.9834; 0.9837; 0.9838)$$

for $\zeta = 1, \gamma = \frac{\sqrt{2}}{2}, \xi = 3.0$

6.3 Surface current densities for TE case

The expressions for the first TE mode of J_{z1} and J_{z2} in (Equation 5.16) and (Equation 5.17), in the same way of to the TM, they are also function of the variable z through a cosine relation:

$$\cos \beta z = \cos \frac{\pi}{b} z$$

So in Figure 18, Figure 19 and Figure 20 the currents as functions of ξ and $\frac{z}{b}$ are reported, in a 3D graph showing the double dependance.

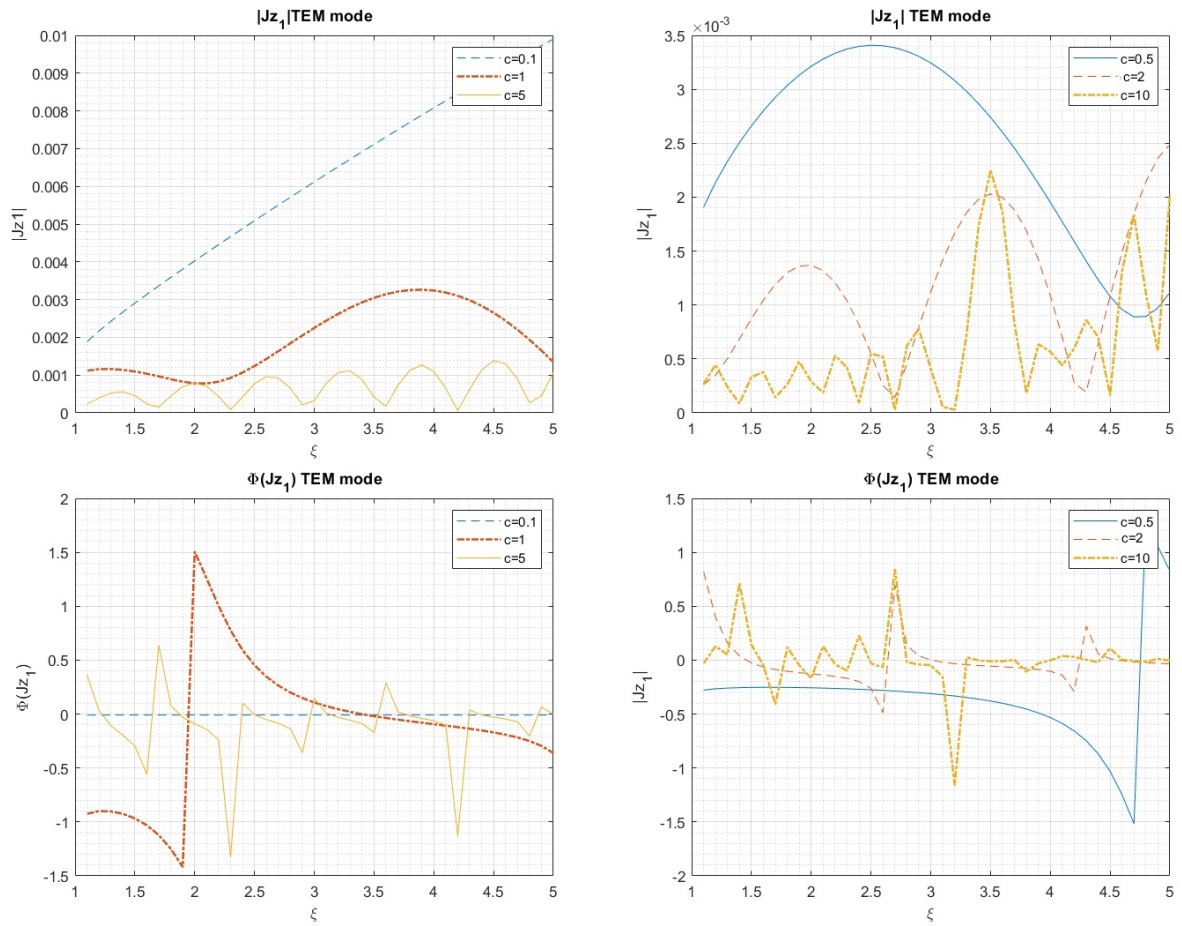


Figure 6: TEM mode: amplitude and phase of J_{z1} for $\zeta = 0.5$:left side for $c = (0.1; 1.0; 5.0)$, right side for $c = (0.5; 2.0; 10.0)$

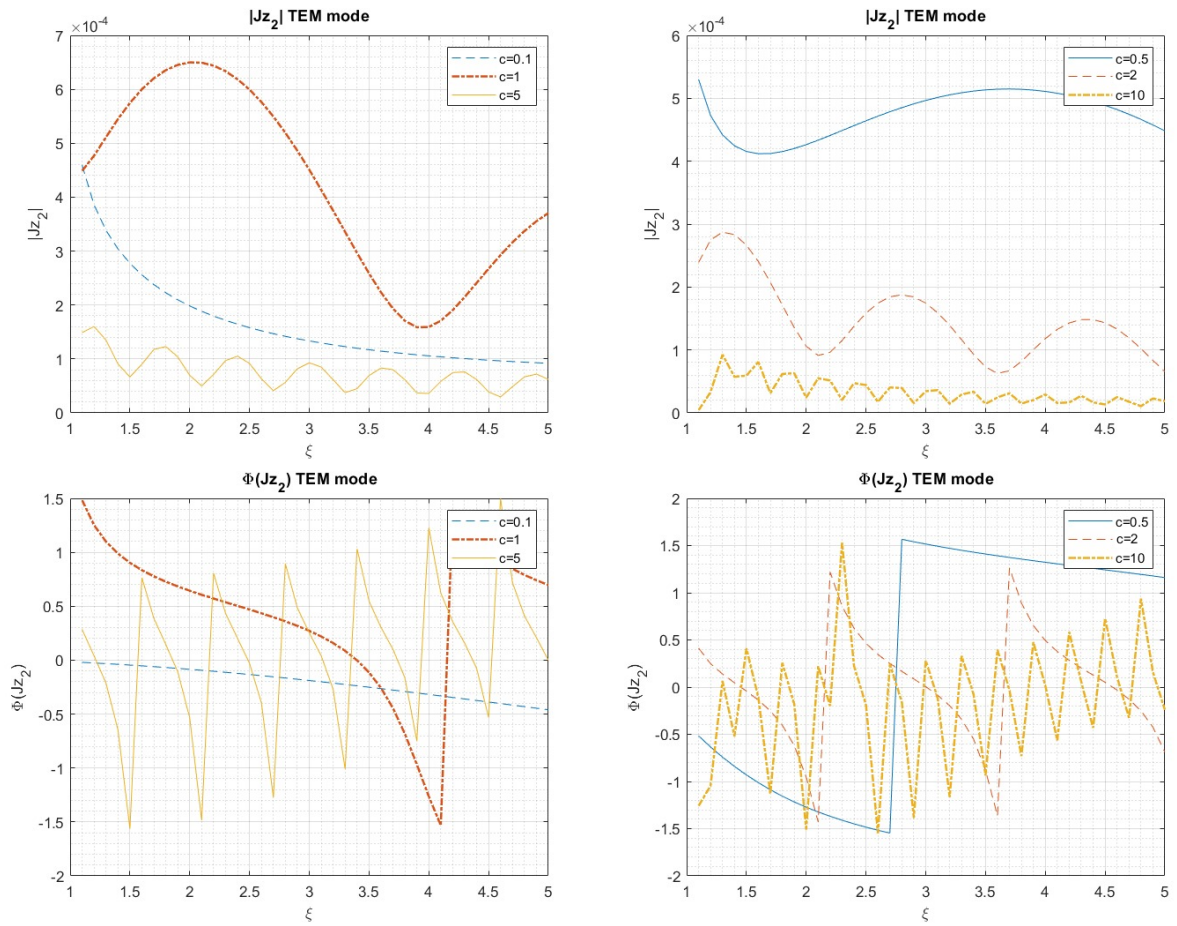


Figure 7: TEM mode: amplitude and phase of J_{z2} for $\zeta = 0.5$: left side for $c = (0.1; 1.0; 5.0)$, right side for $c = (0.5; 2.0; 10.0)$

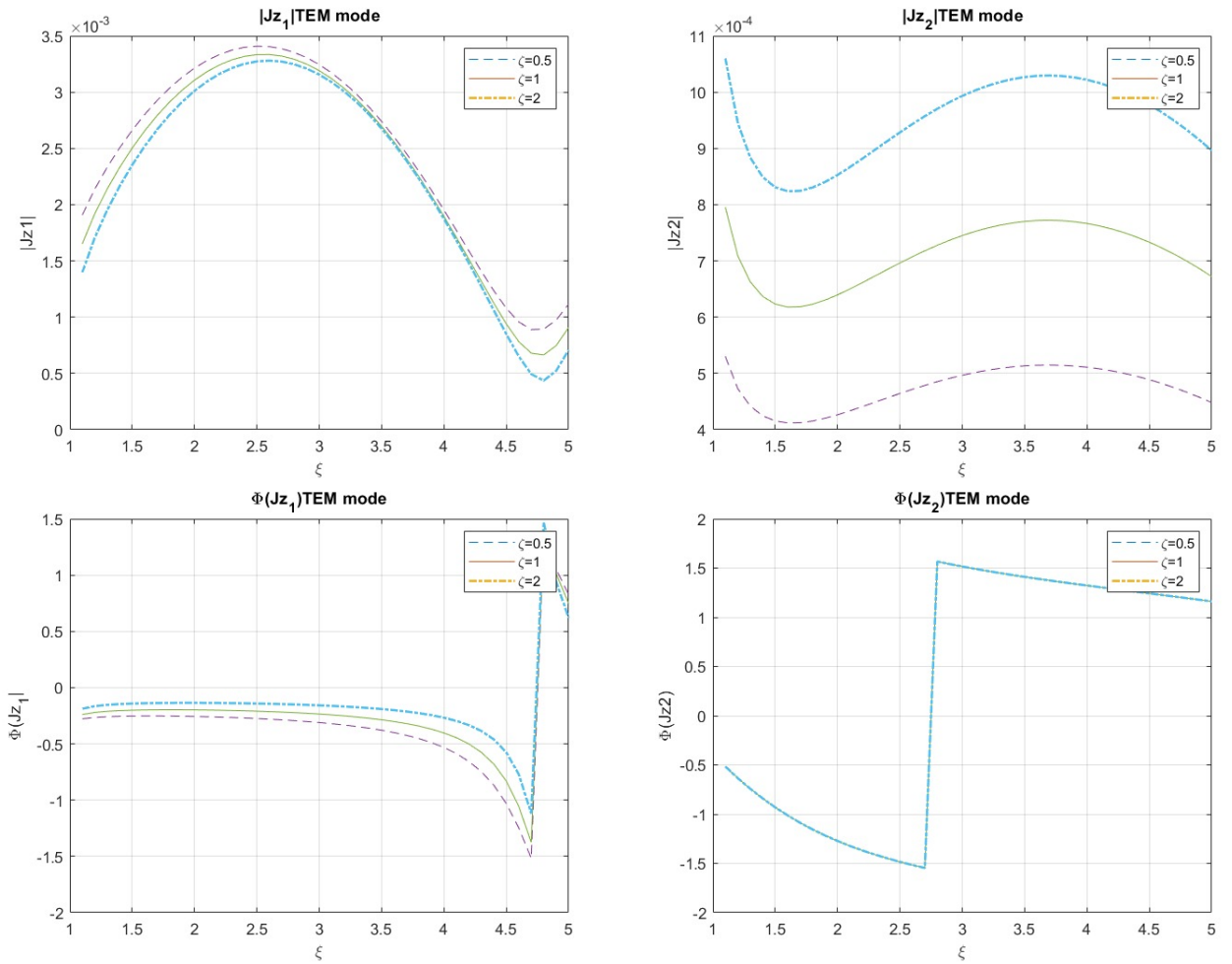


Figure 8: TEM mode: amplitude and phase of J_{z1} (left side) and J_{z2} (right side) for $\zeta = (0.5; 1.0; 2.0)$ and $c = 0.5$

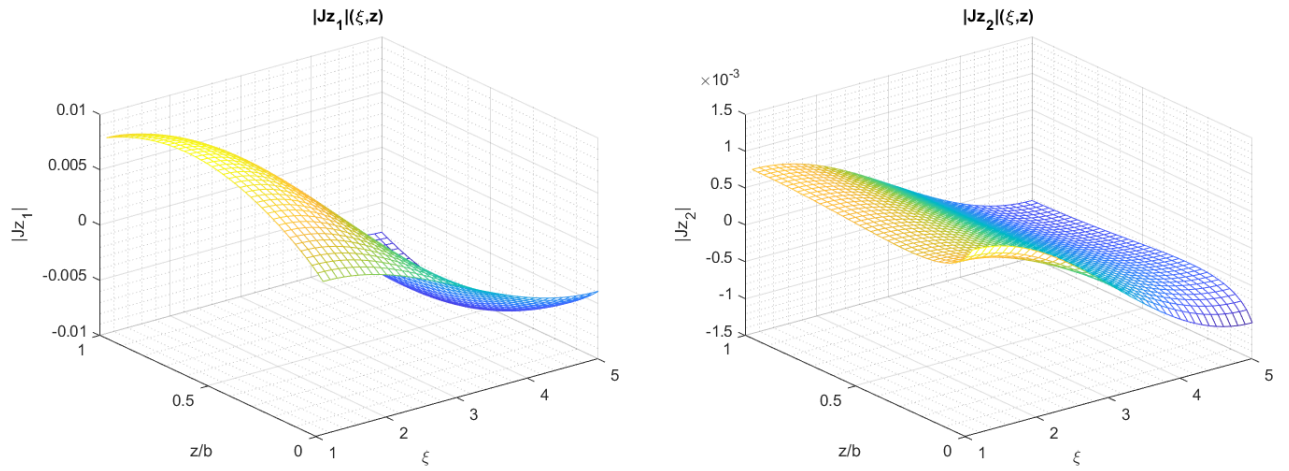


Figure 9: TM mode: amplitude of J_{z1} and J_{z2} w.r.t ξ and $\frac{z}{b}$ with $\zeta = 0.5$ and $\gamma = \frac{1}{2\sqrt{2}}$

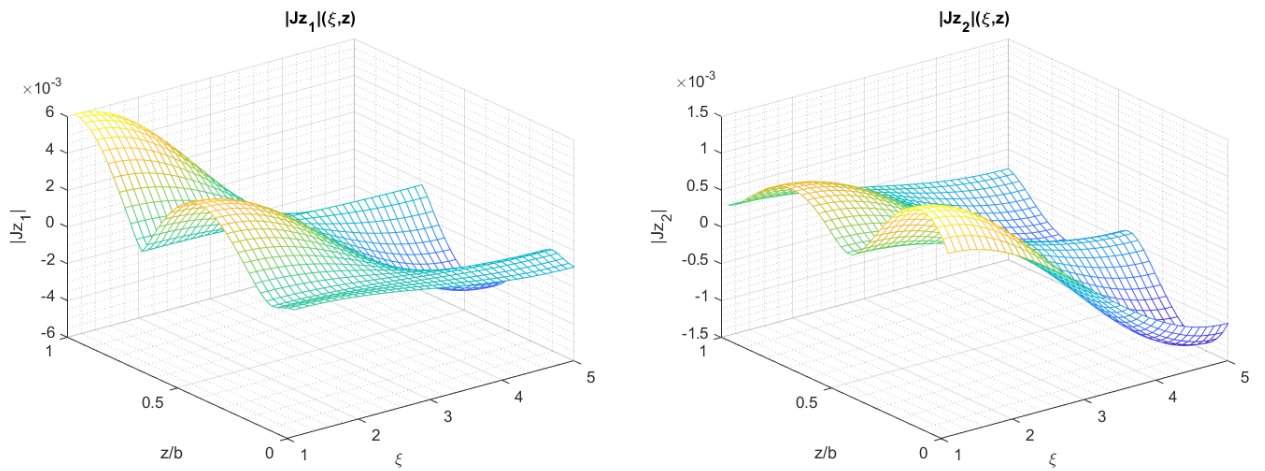


Figure 10: TM mode: amplitude of J_{z1} and J_{z2} w.r.t ξ and $\frac{z}{b}$ with $\zeta = 1$ and $\gamma = \frac{2}{\sqrt{2}}$

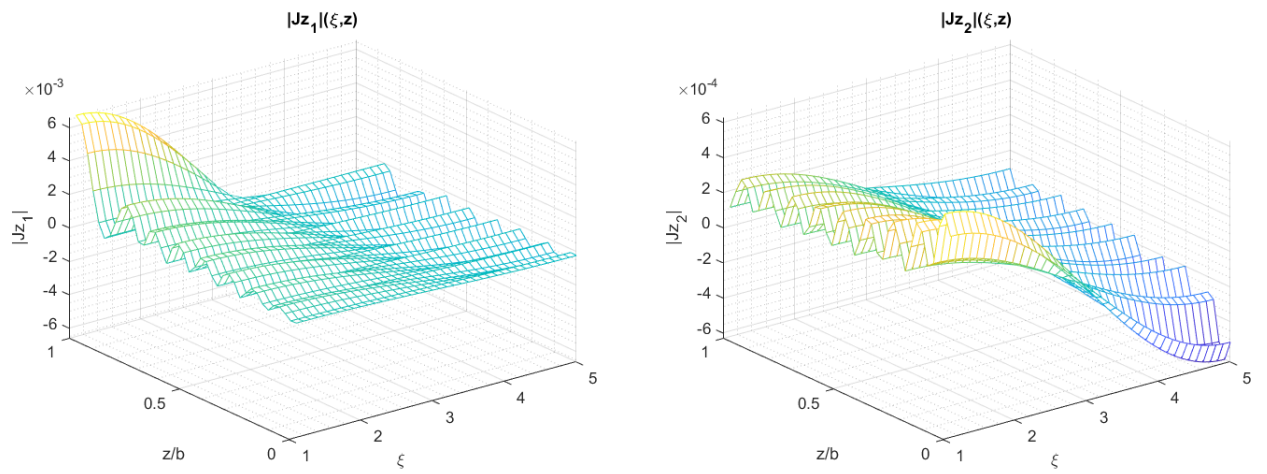


Figure 11: TM mode: amplitude of J_{z_1} and J_{z_2} w.r.t ξ and $\frac{z}{b}$ with $\zeta = 2$ and $\gamma = \frac{10}{\sqrt{2}}$

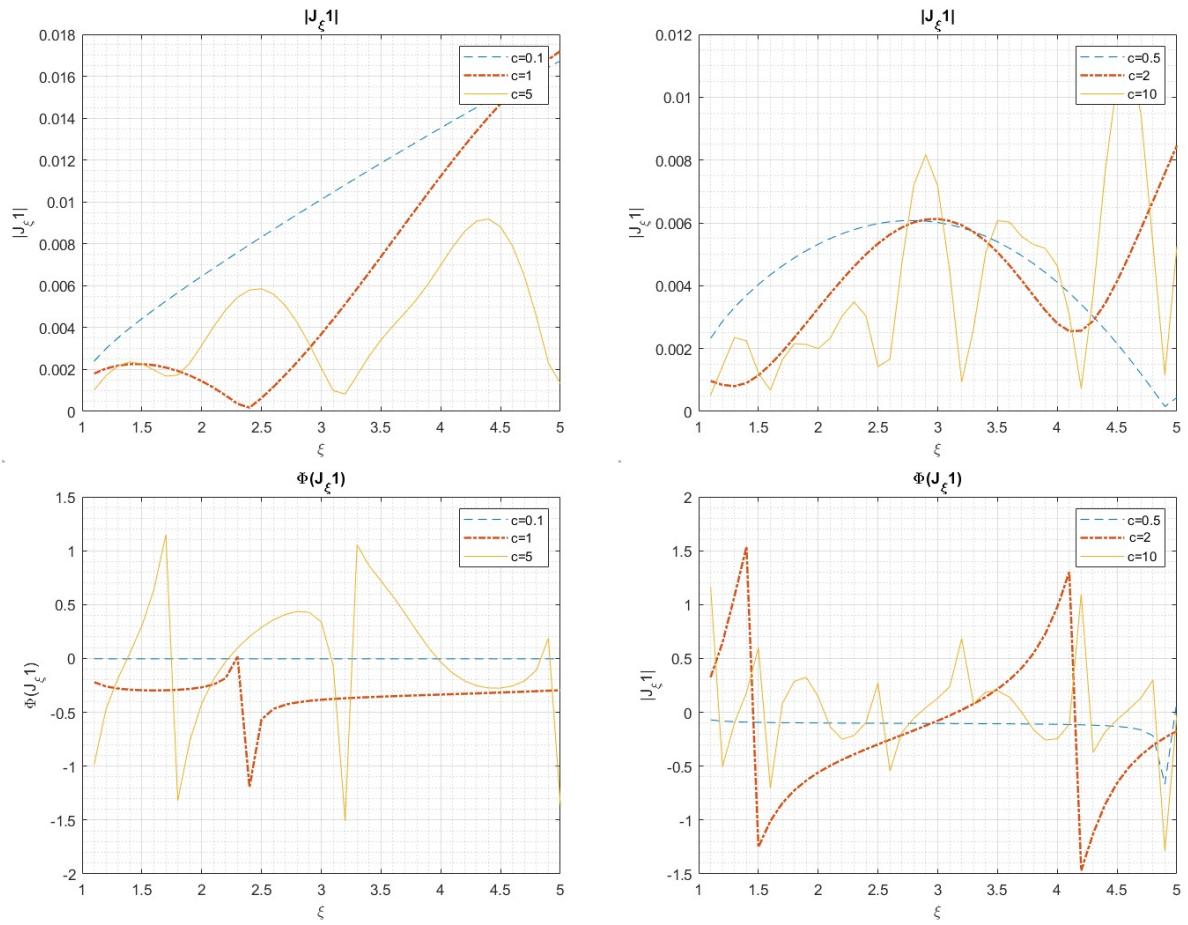


Figure 12: TM mode: amplitude and phase of $J_{\xi 1}$ for $\zeta = 0.5$: left side for $\gamma = (\frac{\sqrt{2}}{20}; \frac{\sqrt{2}}{2}; \frac{5}{\sqrt{2}})$, right side for $\gamma = (\frac{\sqrt{2}}{4}; \sqrt{2}; \frac{10}{\sqrt{2}})$

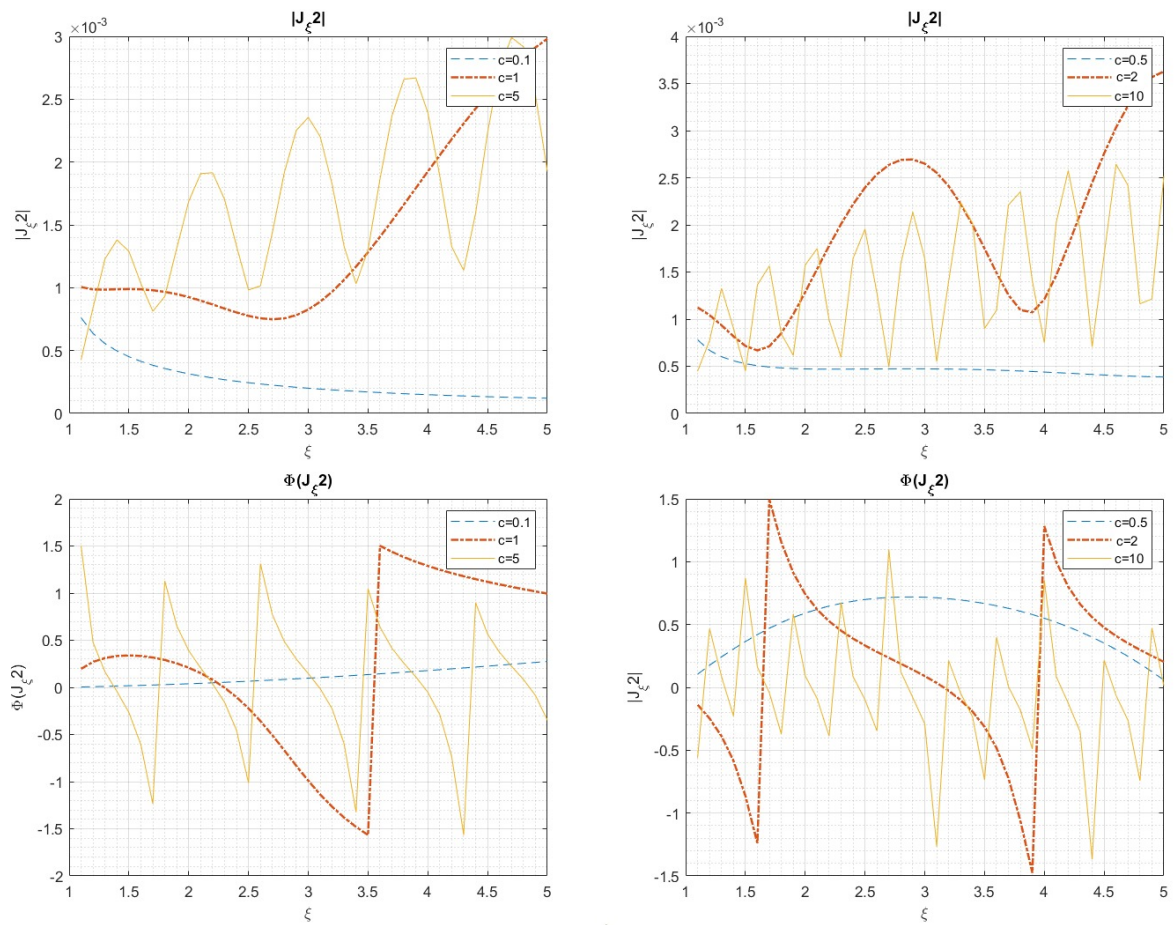


Figure 13: TM mode: Amplitude and phase of $J_{\xi 2}$ for $\zeta = 0.5$: left side for $\gamma = (\frac{\sqrt{2}}{20}; \frac{\sqrt{2}}{2}; \frac{5}{\sqrt{2}})$, right side for $\gamma = (\frac{\sqrt{2}}{4}; \sqrt{2}; \frac{10}{\sqrt{2}})$

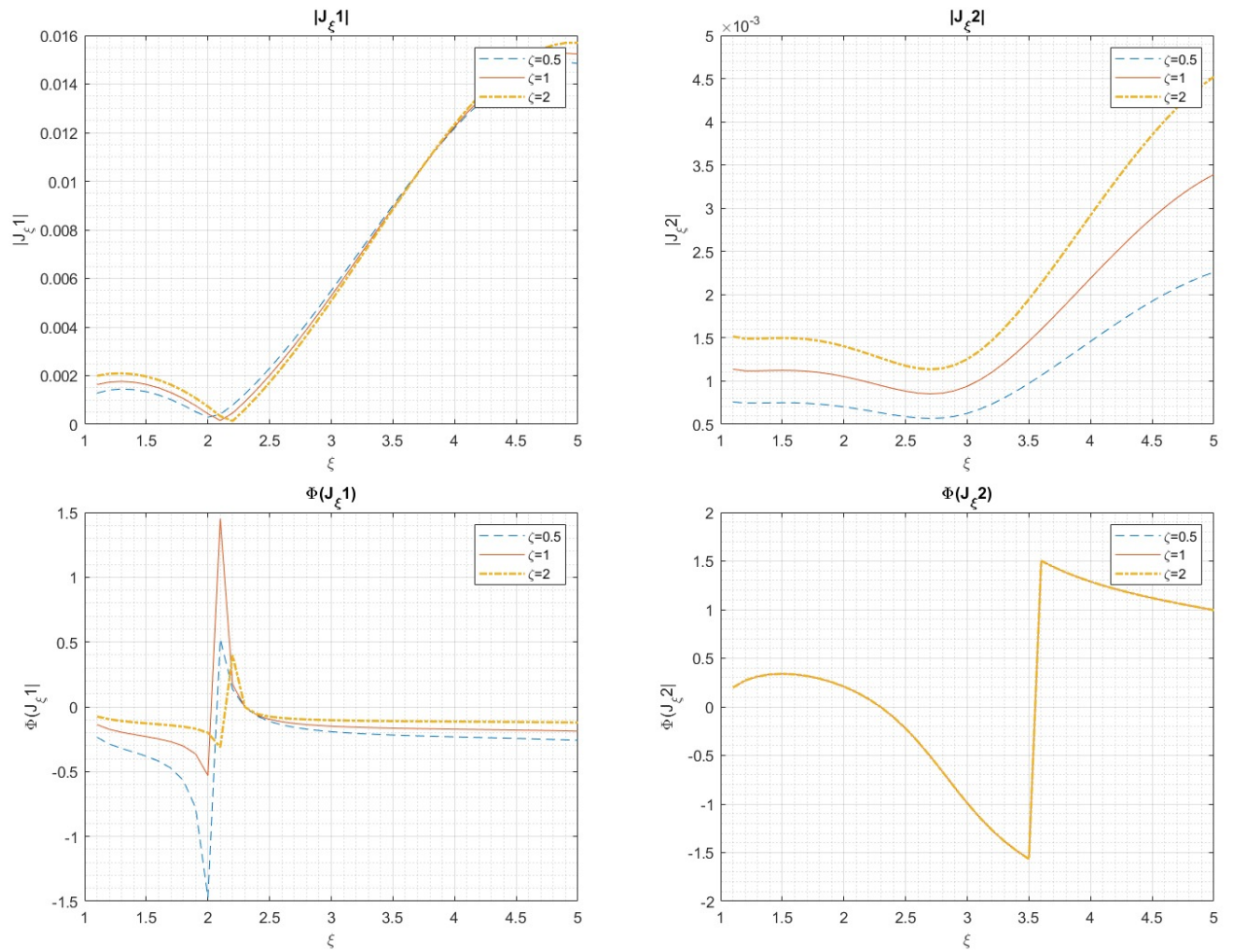


Figure 14: TM mode: amplitude and phase of $J_{\xi 1}$ (left side) and $J_{\xi 2}$ (right side) for $\zeta = (0.5; 1.0; 2.0)$, $\gamma = \frac{\sqrt{2}}{2}$, $\eta = \frac{\sqrt{2}}{2}$

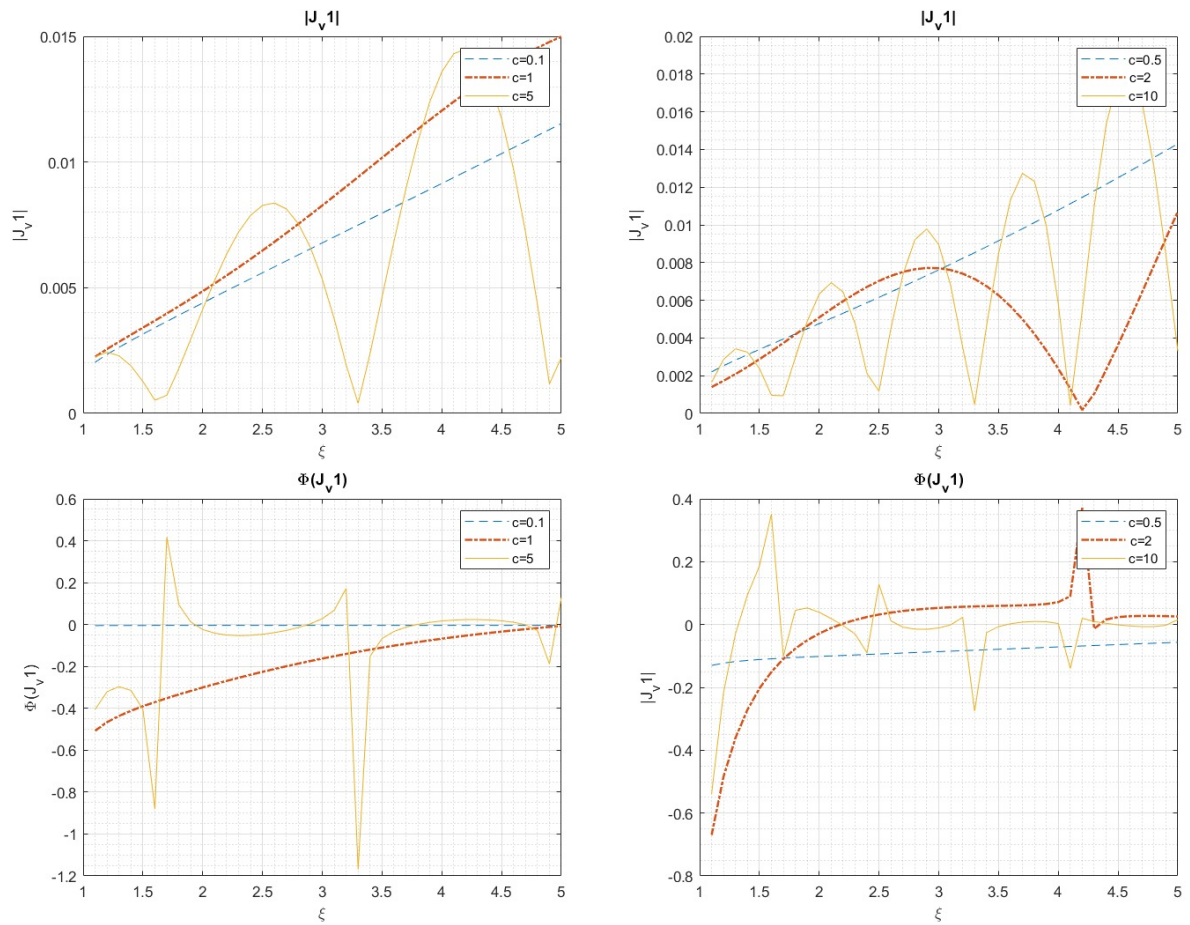


Figure 15: TM mode: amplitude and phase of J_{v1} for $\zeta = 0.5$: left side for $\gamma = (\frac{\sqrt{2}}{20}; \frac{\sqrt{2}}{2}; \frac{5}{\sqrt{2}})$, right side for $\gamma = (\frac{\sqrt{2}}{4}; \sqrt{2}; \frac{10}{\sqrt{2}})$

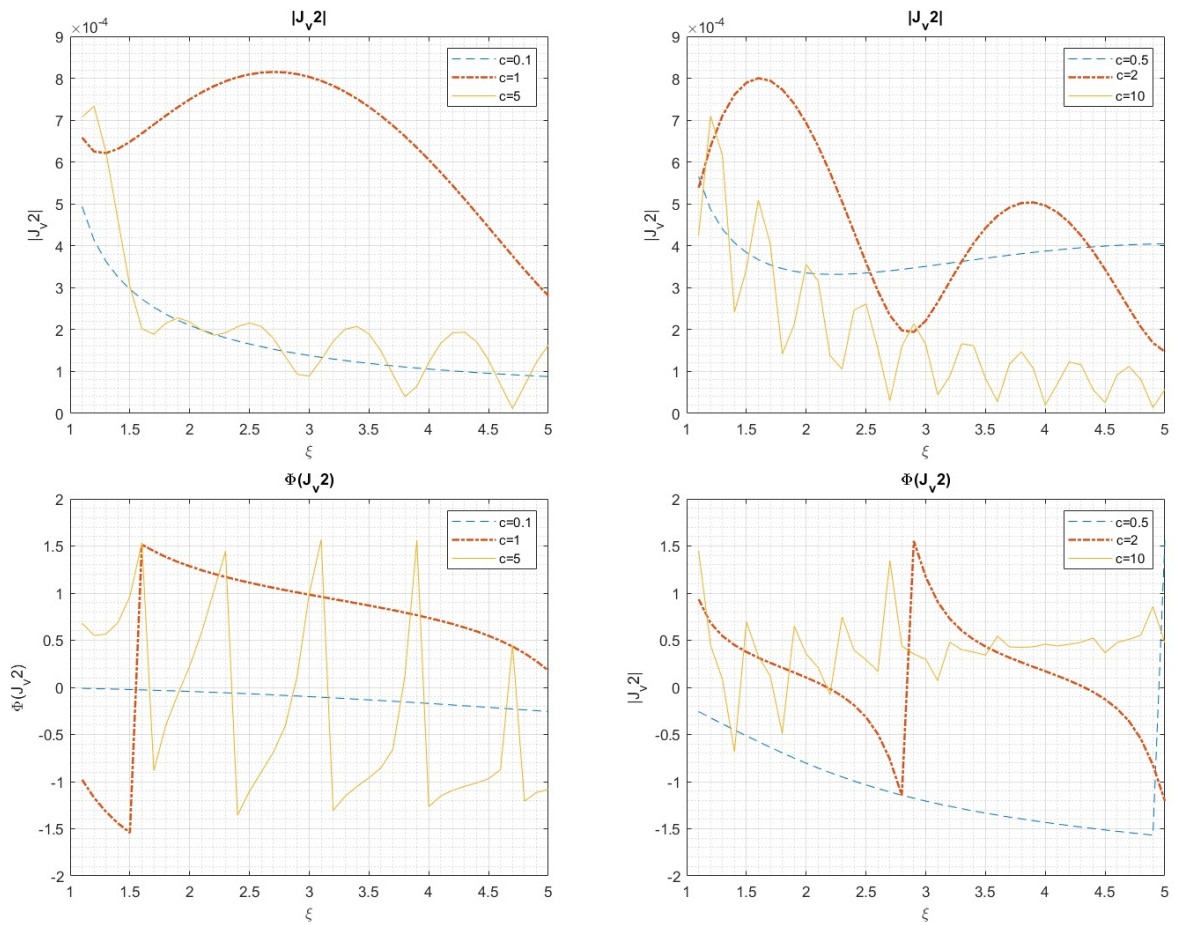


Figure 16: TM mode: Amplitude and phase of J_{v2} for $\zeta = 0.5$: left side for $\gamma = (\frac{\sqrt{2}}{20}; \frac{\sqrt{2}}{2}; \frac{5}{\sqrt{2}})$, right side for $\gamma = (\frac{\sqrt{2}}{4}; \sqrt{2}; \frac{10}{\sqrt{2}})$

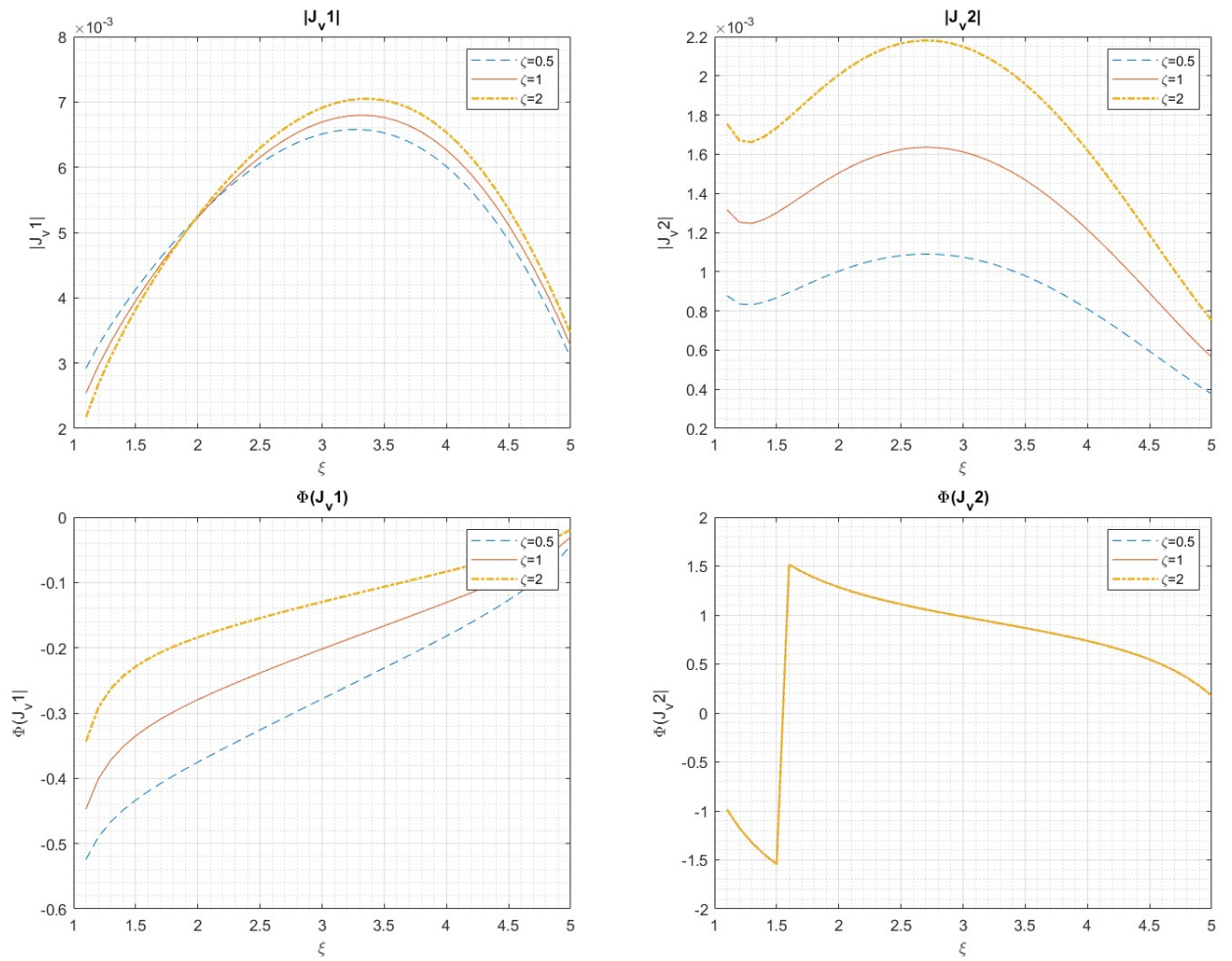


Figure 17: TM mode: amplitude and phase of J_{v1} (left side) and J_{v2} (right side) for $\zeta = (0.5; 1.0; 2.0)$, $\gamma = \frac{\sqrt{2}}{2}$, $\eta = \frac{\sqrt{2}}{2}$

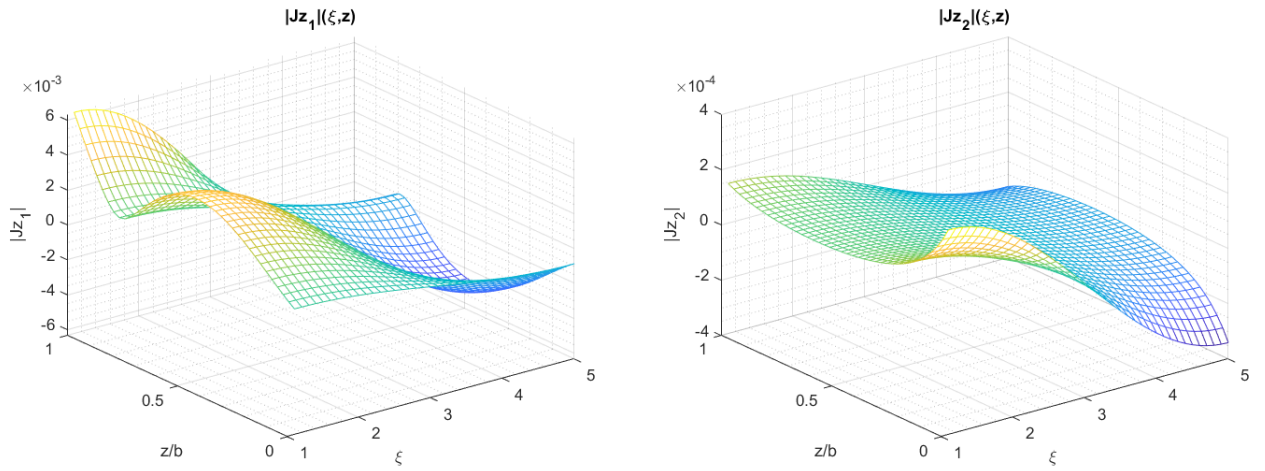


Figure 18: TE mode: amplitude of J_{z1} and J_{z2} w.r.t ξ and $\frac{z}{b}$ with $\zeta = 0.5$ and $\gamma = \frac{1}{2\sqrt{2}}$

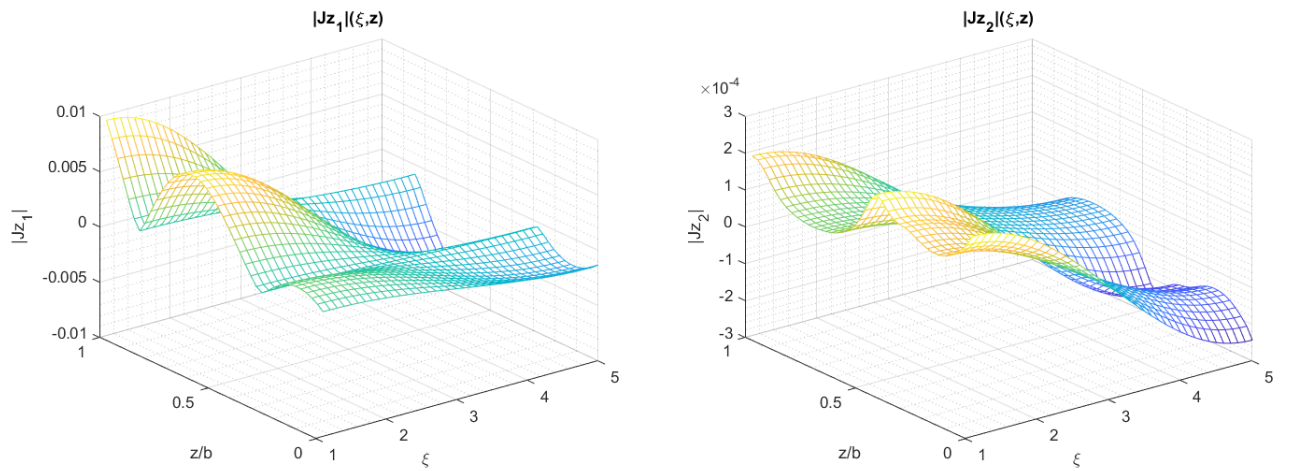


Figure 19: TE mode: amplitude of J_{z1} and J_{z2} w.r.t ξ and $\frac{z}{b}$ with $\zeta = 1$ and $\gamma = \frac{2}{\sqrt{2}}$

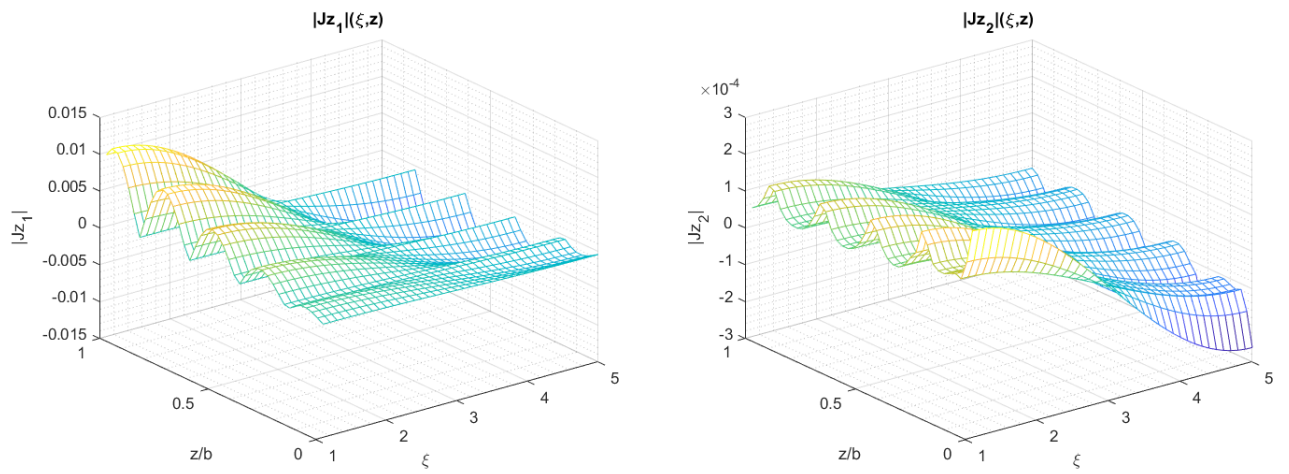


Figure 20: TE mode: amplitude of J_{z_1} and J_{z_2} w.r.t ξ and $\frac{z}{b}$ with $\zeta = 2$ and $\gamma = \frac{5}{\sqrt{2}}$

CHAPTER 7

CONCLUSIONS

A new scattering problem has been presented in this thesis. The analysis is performed considering a parallel-plate waveguide with a slotted wall inserted. Exact solutions, concerning the expression of electric and magnetic field and surface current densities are given for the TEM mode and for the TM and TE modes, using two important results obtained by professor Uslenghi's research. Numerical calculations of some the surface current densities in the various cases are performed with a code developed by professor Erricolo, and the most remarkable results are shown in the graphs.

CITED LITERATURE

1. Uslenghi, P. L.: Exact penetration, radiation, and scattering for a slotted semielliptical channel filled with isorefractive material. IEEE Transactions on Antennas and Propagation, 52(6):1473–1480, 2004.
2. Uslenghi, P. L.: Electromagnetic scattering by metallic cylinders perpendicularly truncated by a metal plane. IEEE Transactions on Antennas and Propagation, 63(5):2228–2236, 2015.
3. Uslenghi, P. L.: Exact scattering by isorefractive bodies. IEEE Transactions on Antennas and Propagation, 45(9):1382–1385, 1997.
4. Stratton, J. A.: Electromagnetic theory. John Wiley & Sons, 2007.
5. Arora, A., Poort, M., and Uslenghi, P.: Scattering by cylindrical posts of various cross sections located inside a parallel-plate waveguide. In URSI National Radio Science Meeting, pages 4–7, 2018.
6. Arora, A.: Electromagnetic Scattering by Various Cylindrical Posts Located Inside a Parallel-Plate Waveguide. Doctoral dissertation, 2018.
7. Erricolo, D.: Algorithm 861: Fortran 90 subroutines for computing the expansion coefficients of mathieu functions using blanchs algorithm. 2006.
8. Erricolo, D. and Carluccio, G.: Algorithm 934: Fortran 90 subroutines to compute mathieu functions for complex values of the parameter. 2013.
9. Erricolo, D.: Acceleration of the convergence of series containing mathieu functions using shanks transformation. IEEE Antennas and Wireless Propagation Letters, 2:58–61, 2003.

VITA

NAME Giorgio Carnevali

EDUCATION

Master of Science in Electrical and Computer Engineering, University of Illinois at Chicago, Dec 2019, USA

Specialization Degree in Analog and Power Electronics , Dec 2019, Polytechnic of Turin, Italy

Bachelor degree in Electronic and Communication engineering, Dec 2016 Universita' Politecnica delle Marche, Italy

LANGUAGE SKILLS

Italian Native speaker

English fluent

2017 - IELTS examination (6.5/9)

A.Y. 2018/19 One Year of study abroad in Chicago, Illinois

A.Y. 2017/18. Lessons and exams attended exclusively in English

SCHOLARSHIPS

Spring 2019 Italian scholarship for final project (thesis) at UIC

Fall 2018 Italian scholarship for TOP-UIC students
